Opto-Electronic Science

CN 51–1800/O4 ISSN 2097–0382 (Print) ISSN 2097–4000 (Online)

Dynamic spatial beam shaping for ultrafast laser processing: a review

Cyril Mauclair, Bahia Najih, Vincent Comte, Florent Bourquard and Martin Delaigue

Citation: Mauclair C, Najih B, Comte V, et al. Dynamic spatial beam shaping for ultrafast laser processing: a review. *Opto-Electron Sci* **4**, 250002 (2025).

https://doi.org/10.29026/oes.2025.250002

Received: 15 January 2025; Accepted: 24 March 2025; Published online: 6 June 2025

Related articles

High-frequency enhanced ultrafast compressed active photography

Yizhao Meng, Yu Lu, Pengfei Zhang, Yi Liu, Fei Yin, Lin Kai, Qing Yang, Feng Chen

Opto-Electronic Advances 2025 **8**, 240180 doi: 10.29026/oea.2025.240180

High performance micromachining of sapphire by laser induced plasma assisted ablation (LIPAA) using GHz burst mode femtosecond pulses

Kotaro Obata, Shota Kawabata, Yasutaka Hanada, Godai Miyaji, Koji Sugioka

Opto-Electronic Science 2024 **3**, 230053 doi: 10.29026/oes.2024.230053

Three-dimensional isotropic microfabrication in glass using spatiotemporal focusing of high-repetition-rate femtosecond laser pulses

Yuanxin Tan, Haotian Lv, Jian Xu, Aodong Zhang, Yunpeng Song, Jianping Yu, Wei Chen, Yuexin Wan, Zhaoxiang Liu, Zhaohui Liu, Jia Qi, Yangjian Cai, Ya Cheng

Opto-Electronic Advances 2023 **6**, 230066 doi: 10.29026/oea.2023.230066

Applications of lasers: A promising route toward low-cost fabrication of high-efficiency full-color micro-LED displays

Shouqiang Lai, Shibiao Liu, Zilu Li, Zhening Zhang, Zhong Chen, Rong Zhang, Hao-Chung Kuo, Tingzhu Wu

Opto-Electronic Science 2023 **2**, 230028 doi: 10.29026/oes.2023.230028

Opto-Electronic Science

Review

xxxx 2025, Vol. x, No. x

DOI: 10.29026/oes.2025.250002 CSTR: 32246.14.oes.2025.250002

Dynamic spatial beam shaping for ultrafast laser processing: a review

Cyril Mauclair[1]*, Bahia Najih[2,3], Vincent Comte[4,5], Florent Bourquard[2] and Martin Delaigue[3]

This review examines the state-of-the-art in spatial manipulation of ultrafast laser processing using dynamic light modulators, with a particular focus on liquid crystal-based systems. We discuss phase modulation strategies and highlight the current limitations and challenges in surface and bulk processing. Specifically, we emphasize the delicate balance between high-fidelity beam shaping and energy efficiency, both critical for surface and bulk processing applications. Given the inherent physical limitations of spatial light modulators such as spatial resolution, fill factor, and phase modulation range. We explore techniques developed to bridge the gap between desired intensity distributions and actual experimental beam profiles. We present various laser light modulation technologies and the main algorithmic strategies for obtaining modulation patterns. The paper includes application examples across a wide range of fields, from surgery to surface structuring, cutting, bulk photo-inscription of optical functions, and additive manufacturing, highlighting the significant enhancements in processing speed and precision due to spatial beam shaping. The diverse applications and the technological limitations underscore the need for adapted modulation pattern calculation methods. We discuss several advancements addressing these challenges, involving both experimental and algorithmic developments, including the recent incorporation of artificial intelligence. Additionally, we cover recent progress in phase and pulse front control based on spatial modulators, which introduces an extra control parameter for light excitation with high potential for achieving more controlled processing outcomes.

Keywords: spatial light modulator; ultrafast laser processing; spatial beam shaping; laser surface structuring; laser bullk structuring

Mauclair C, Najih B, Comte V et al. Dynamic spatial beam shaping for ultrafast laser processing: a review. *Opto-Electron Sci* **x**, 250002 (2025).

Introduction

The use of ultrafast laser pulses for surface and bulk processing is a technique that has now several applications due to the high degree of structuring precision because of its particular light-matter interaction with low thermal side-effects[1,2]. The field has known a recent change of paradigm with the development of Ytterbium-based laser sources and amplifiers with scalable architectures[3,4] that allowed for high power and high pulse repetition rates with a much higher degree of stability than the historical Ti:Sa based platform[5–67].

This technological breakthrough has opened many doors for biomedical and industrial applications as power and speed (i.e repetition rate) of the laser sources are not anymore the main limitations to most of the processing

[1]Université d'Angers, LPHIA, SFR MATRIX, 49000 Angers, France; [2]Laboratoire Hubert Curien, UMR 5516 CNRS, Université Jean Monnet, 42000 Saint-Étienne, France; [3]Amplitude, 33600 Pessac, France; [4]Laboratoire BiiO, Université Jean Monnet, 42000 Saint-Étienne, France; [5]Keranova, 42000 Saint-Étienne,France.

*Correspondence: C Mauclair, E-mail: cyril.mauclair@univ-angers.fr

Received: 15 January 2025; Accepted: 24 March 2025; Published online: 6 June 2025

applications. Indeed, the current main question is how to handle so many and so intense pulses in an effective way? Most of the time, micro processing applications do not require more than a few μJ per pulse (eye surgery[8,9], surface or bulk nano or microstructuring[10,11], ablation[12,13], glass sculpting[14], bulk photoinscription[15], photopolymerisation[16] etc.). Higher pulse energy often lead to unwanted side effects either within the processed area or along the beam propagation path before reaching the target. In the first case, too large pulse energies decrease the material removal efficiency (the ratio of the ablated mass with respect to the number of photons)[17] and may add chaotic surface structuring[18,19]. Similar problems are encountered in bulk processing where uncontrolled cracking can occur[20]. In the second case, beam deformation may take place in air when a focused region is necessary before reaching the target or within the bulk when focusing inside transparent materials[21,22].

High repetition rates also constitute a challenge by themselves. The high degree of processing precision associated with ultrafast pulses is mainly related to a light-matter interaction with a much lower onset of thermal effects than in the case of longer laser pulses[12,23]. When sending pulses at MHz repetition rates or more, thermal relaxation between pulses is no longer ensured even on metals leading to uncontrolled structuring on surfaces and inside transparent materials[24,25]. We note here that sometimes, melted and re-solidified structures can be of interest to confer specific properties to the surface, like hydrophobicity[26] but also to accelerate the process of percussion drilling[27]. However, high repetition rate management usually consists in very high speed scanning of the laser spot to reduce the pulse spatial overlap on the target. This is now a bottleneck of femtosecond surface processing, leading to the developments of high deflection speed polygonal scanners[28,29], or electro/acousto-optic scanners[30]. Let us mention here that even higher repetition rates (of a few GHz and above) lead to phenomena where enhanced ablation is achieved with low onset of side thermal effects, refereed to as the ablation-cooled regime[31,32]. In this regime however, the most efficient ablation and milling regimes are usually accompanied with lower surface quality, requiring additional low pulse energy processing[33].

Apart from high speed scanning, the alternate and complimentary strategy to maintain proper processing conditions with high energetic and high repetition rate laser sources is to adapt the beam intensity distribution to the adequate fluence level. Most of the time, the laser beam is quite strongly attenuated with half waveplate and polarizer and filters[2]. If the technique is simple and efficient for experimental research, it is obvious that such an additional waste of energy is simply not acceptable for industrial application; especially considering the very low energy efficiency of high power lasers[4,34].

Let us recall that laser spot enlarging to decrease the peak intensity towards the adequate fluence can be performed using lenses or parabolic mirrors. However this techniques obviously augments the laser spot size and thus the interaction area. As a consequence, it cannot by applied to many ultrafast laser processing applications where a typical micrometric spatial structuring resolution is required. This is where dynamic spatial beam shaping comes to play[35–37]. By sculpting the laser intensity distribution in a quasi-arbitrary manner (with some limitations that will by addressed later), both precision and proper fluence levels can be combined. In the following, we strive to give a rather complete picture of the technique of dynamic spatial beam shaping in ultrafast processing. An emphasis on liquid crystal based spatial phase modulators is given due to their intrinsic advantage of dynamic reconfigurability and high laser energy efficiency.

After describing the current state of the art of the commercially available light modulators with their development trends and limitations, we present the main strategies currently used for light modulation pattern calculation and discuss their shortcomings when it comes to the experimental implementation. An overview of applications in a wide variety of fields is then given with a particular effort to confront some results with the technological and algorithmic limitations. After that, we review some applications of spatial beam shaping involving precision surface structuring and bulk structuring. The generation and use of non-diffractive beams for drilling and cutting is then addressed followed by vortex beam shaping and spatial polarization shaping. We then discuss additive manufacturing applications taking advantage of spatial beam shaping. The latest algorithmic and experimental improvements are also revised with an emphasis on feedback assisted optimization loops and artificial intelligence computation strategies. In some cases, these progresses are not directly related to laser processing applications, but the attained level of performance triggers a strong interest for the topic of this review. Finally, recent results concerning spatiotemporal

effects involving pulse front control are described due to their strong potential of excitation localization control in ultrafast laser processing.

Basics of dynamic spatial beam shaping

An historical example of spatial beam control can be found in the report of the siege of Syracuse 212 BC. Following Archimedes instructions, numerous parabolic reflective surfaces (probably polished shields of Cu or bronze) were positioned to redirect and focus the light rays from the sun onto the Roman fleet boats. Interestingly, the experience was repeated by a group of students of the MIT in october 2005. Fire ignition was obtained on wood[38]. The city was eventually invaded by the Romans, as a very early proof of the fact that spatial beam control requires careful developments and optimizations to reach its target.

Much more recently, it is interesting to note that the keywords 'beam shaping' and 'laser beam shaping' have known a continuous gain of utilization inf scientific articles over the last twenty years, with a doubling occurrence factor between 1990 and 2020 (extraction from Google Scholar database using the Python script in ref.[39]). When handling a light beam emitted from a stable laser cavity, the spatial intensity repartition of the fundamental mode detected in a given plane $I(x,y)$ is most of the time represented by a Gaussian distribution. In the frame of the paraxial approximation (i.e the transverse beam dimensions remain small enough compared to propagating distances), a quite famous solution to the scalar wave equation designed to represent laser emission is the Gaussian beam[40]. Thus, $\tilde{u}(x,y,z)$ takes then the form:

$$\tilde{u}(x,y,z) = \frac{u_0}{q(z)}\exp\left(-\mathrm{i}k\frac{x^2+y^2}{2q(z)}\right), \qquad (1)$$

where

$$\frac{1}{q(z)} = \frac{1}{R(z)} - \frac{\mathrm{i}\lambda}{\pi w^2(z)} = \frac{1}{q_0+z}, \qquad (2)$$

$R(z)$ is the wavefront radius of curvature. It is worth noting the z dependency, meaning that any beam modulation in amplitude or in phase has a consequence in the transverse plane and along the propagation axis. $w(z)$ is the beam radius at $\frac{1}{\mathrm{e}^2}$ of the intensity profile $I(x,y,z) = \tilde{u}(x,y,z)\times\tilde{u}(x,y,z)^\star$ which follows a Gaussian distribution. $q(z)$ is the complex beam parameter. This quantity allows for a complete spatial definition of the Gaussian beam with the relation $q(z) = q_0 + z$. Taking the origin of the z-axis at $z = 0$ at the waist position $w(z) = w_0$ we have $R(z) = \infty$ meaning that at this point the wavefront is a plane orthogonal to the propagation axis (although not to be confused with a plane wave[41]).

From these equations, it can been seen that any modulation of amplitude and/or wavefront in a given x-y plane has an impact on the subsequent laser intensity distribution in further x-y planes and along the z axis. For example, if a laser beam goes through a converging lens of focal length f, the corresponding parabolic wavefront modulation can be taken into account by adding the phase term $\phi_f = -\mathrm{i}\pi\frac{x^2+y^2}{\lambda f}$ in the exponential of Eq. (1). This modulation enters in competition with the intrinsic divergence of the Gaussian beam wavefront represented by the term $-\mathrm{i}k\frac{x^2+y^2}{2q(z)}$. Thus, the lens alters the beam size, ultimately leading to a focal spot at the position $z = f$. More generally, if the laser beam encounters any spatial phase modulation ϕ_M or any amplitude modulation, those can be mathematically applied by a factor to Eq. (1) with consequences on the propagated laser beam profile.

Following ref.[42], within the paraxial approximation and neglecting spectral effects, the transverse intensity profile $I(x',y')$ after propagation over the distance D of a Gaussian laser field of amplitude $\tilde{A}(x,y)$ focused by a lens of focal distance f is defined by:

$$I(x',y') \propto \left|\mathcal{F}_{fx',\,fy'}\left[\tilde{A}(x,y)\mathrm{e}^{-\phi_D+\phi_f+\phi_{\mathrm{Ab}}+\phi_M}\right]\right|^2, \qquad (3)$$

where $\mathcal{F}_{fx',\,fy'}$ is the two-dimensional (2D) Fourier transform with respect to the spatial frequencies in the (x',y') plane, λ is the laser wavelength, $\phi_D = \mathrm{i}\pi\frac{x^2+y^2}{\lambda D}$ is the phase term corresponding to the beam propagation over D, ϕ_{Ab} comprehends the optical aberrations and ϕ_M stands for the phase modulation purposely added on the beam path to control $I(x',y')$. Usually, this plane of interest is the focal plane of a lens or a focusing element, where both the maximum of intensity and ultimate resolution can be reached. This focal intensity distribution in and around the focal plane can be computed from Eq. (2) using the fast Fourier transforms (FFT) readily available in many computing languages[42]. The concept of ultrafast laser beam shaping is illustrated by Fig. 1. By tuning the amplitude and/or the wavefront of the laser before the focusing element, it is possible to control the focal intensity distribution. Amplitude modulation techniques

have shown interesting results for ultrafast laser processing with relatively simple experimental apparatus like slit shaping for bulk transverse waveguide photoinscription[43], iris imaging for surface structuring[21] or more advanced set-up involving dynamic reconfigurability[44]. However, the amplitude modulation inevitably implies a significant loss of laser energy in the blocked parts of the beam. Thus, we focus in the following on wavefront modulation, a technique that potentially preserves all the laser energy which is required for efficient surface or bulk processing. Phase modulation masks are placed on the ultrafast laser beam path and permit to shape the focal intensity distribution by generating arrays of spots, changing the spot shape or controlling the beam diffraction around the focal plane as illustrated in Fig. 1. The light modulator device allows for dynamic changes of the wavefront modulation ϕ_M that can be operated during laser processing giving a higher degree of efficiency and flexibility to the process.

Let us briefly precise that this report considers light pulses whose spectral bandwidth can be assumed thin enough so that any chromatic aberration can be disregarded in a first approximation (the situation will be different in Section *Perspectives offered by spatio-temporal* where spatiotemporal effects will be considered). When dealing with ultrafast laser pulses from Ti:Sa lasers at 800 nm, the spectral bandwidth can be as large as 100 nm for a Fourier-limited 10 fs pulse (i.e a pulse whose spectral components are not temporally spread[41]). In the other way around, 100 fs pulses carry a 10 nm spectral bandwidth. Let us consider a simple converging lens. The chromatic aberrations implies that rays associated with the redder part of the spectrum are focused further than the bluer one. Given the focal length f of a lens of refractive index n, the axial spreading Δf around F along the propagation axis writes:

$$\frac{\Delta f}{f} = \frac{\Delta\lambda}{\lambda}\frac{\Delta n}{n-1}, \tag{4}$$

with $\Delta\lambda \approx 10$ nm being the laser source relatively narrow spectral bandwidth centered on 800 nm and Δn the refractive index difference for the boundary wavelength of the laser spectrum obtained from the Sellmeier relations[45]. For a fused silica lens, $\frac{\Delta f}{f} = 4.8 \times 10^{-6}$,

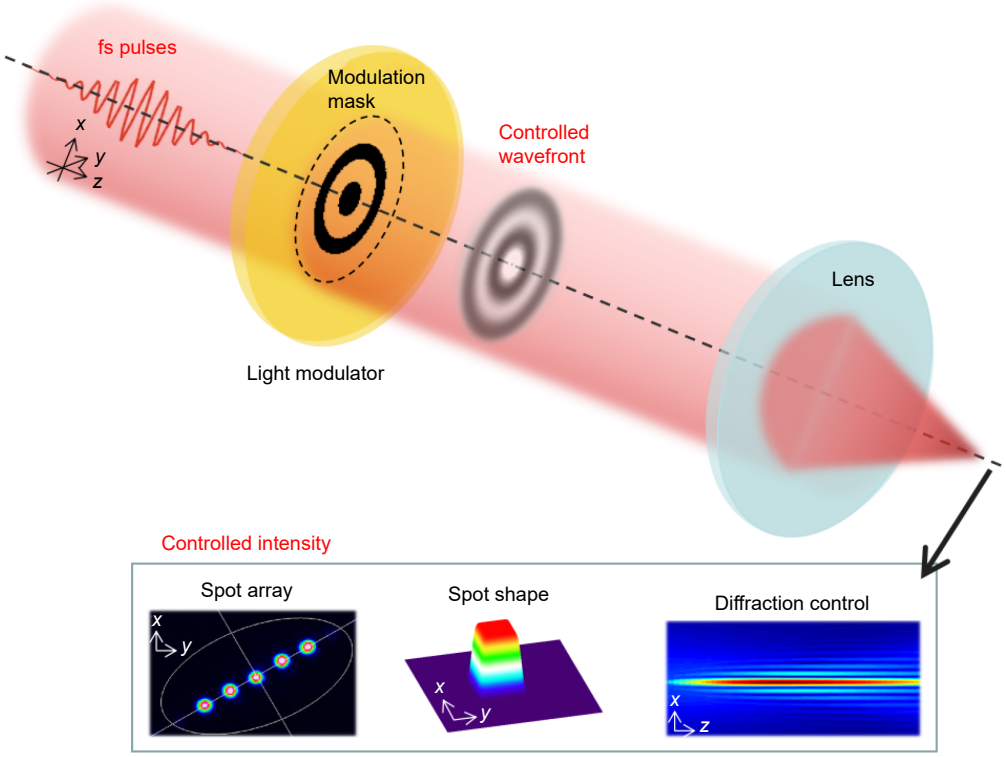

Fig. 1 | Principle of spatial beam shaping of ultrafast laser. A light modulator (transmittive or reflective) is placed on the laser beam path. It imprints a wavefront modulation (modulation mask) that rearranges the laser intensity distribution in a further plane of propagation, usually the focal plane of a converging element. There, a variety of beam distributions can be obtained in he three dimensions, from multi-spot arrangement to continuous beam shapes, as well as non-diffracting beams.

corresponding to a few nanometers in the case of a focal length of $f = 1$ cm which is clearly negligible compared to the micrometric dimensions of the focal intensity distribution. In this latter case and for even thinner spectral bandwidth (e.g Ytterbium-based ultrafast laser with $\Delta\lambda$ below 7 nm and $\approx$ 300 fs pulse duration), it is thus quite reasonable to neglect the effect of chromatic aberration. This being said, research efforts have focused on adapting spatial beam shaping techniques to accommodate large spectral bandwidth ultrafast pulses. The strategy involves using consecutive diffractive optical elements for successive beam shaping planes, followed by dispersion-related compensation[46,47]. Additionally, it is noteworthy that wavefront shaping with intensity feedback can mitigate these types of non-uniformities, requiring only a single reconfigurable wavefront shaper[48].

Dynamic spatial beam shaping apparatus

Dynamic wavefront modulation for spatial beam shaping can be performed through several techniques, we have retained 5 of them that present interesting performances and are well-known to the community.

Spatial light modulators (SLM) based on a liquid crystal layer are widespread components in photonics with a large variety of applications including laser processing, imaging, communications (refer to an interesting review here[49]). They have triggered much attention in the field of laser processing[50] and significantly enhanced the capabilities of ultrafast laser processing[51]. As illustrated in Fig. 2(a)), the LC layer can act as a dynamic phase retardation map thanks to the possibility to orientate the LC molecules with a local electric field. The principle is applicable in reflection or in transmission with a photoconductive material[52]. The SLM technology has known remarkable advances in terms of resolution and fill factor[49] allowing for more controlled beam shapes. Their typical pixel size is now below 5 μm with 4*k* definition and a refresh rate of 50–100 Hz commercially available. The phase range is usually 2π. Power handling and response time are the two main directions of developments[53,54],

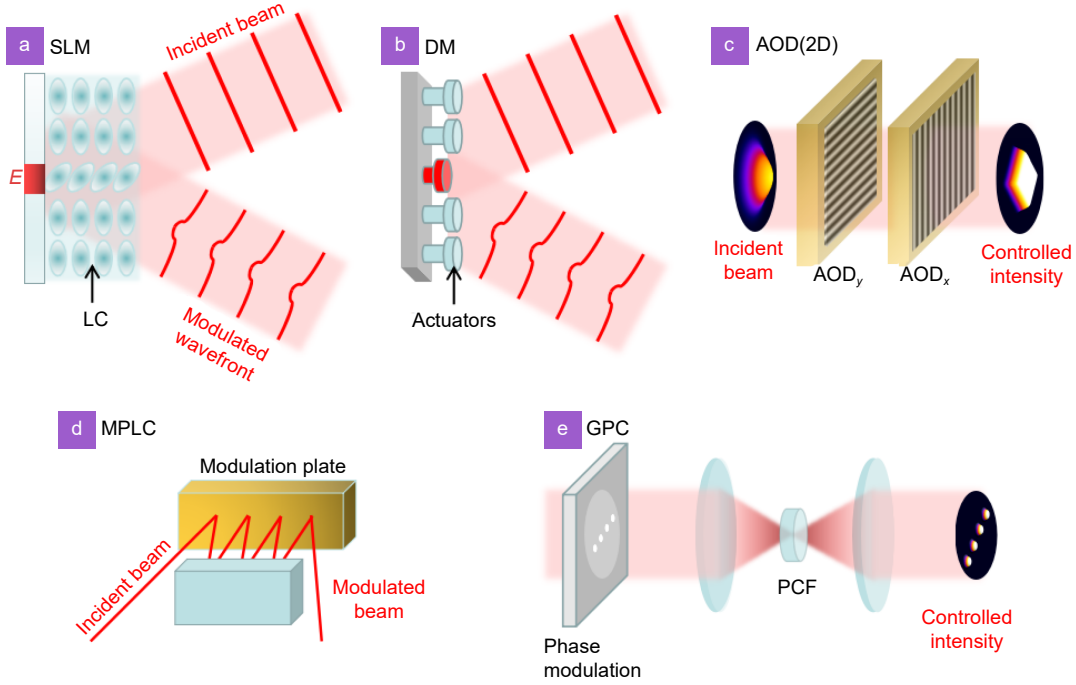

Fig. 2 | Main experimental systems for dynamic wavefront modulation. (**a**) Spatial light modulators (SLM) are based on a liquid crystal (LC) layer whose molecules can be orientated under an electric field *E*, permitting to dynamically control the spatial optical retardation of an impinging laser beam. (**b**) Deformable mirrors (DM) rely on a similar principle with actuators whose controllable height defines the optical retardation on the beam wavefront. They can be membrane-based or segmented. (**c**) The acousto-optic deflectors (AOD) are based on the generation of sound waves inside a crystal (e.g. TeO_2 or $PbMoO_4$). The related periodical variation of refractive index also permits wavefront modulation. (**d**) The multi-plane light conversion (MPLC) set-up is based on spatial mode conversion through successive passages on specifically designed phase retardation maps. (**e**) The general phase contrast method (GPC) relies on the principle of phase contrast microscopy where the transparent pure-phase sample corresponds to a controlled phase modulation (applied with an SLM for example) and the phase contrast filter (PCF) is the optical element turning this modulation into an intensity contrast in an imaging plane. See text for more details.

noteworthily following the advances of ultrafast laser systems in terms of average power and repetition rates.

Deformable mirrors (DM) are very well-known devices used in adaptive optics to correct for geometrical aberrations. As illustrated in Fig. 2(b)), controlling the height of a series of actuators permits to modulate the laser wavefront reflected on the device. The DMs can be membrane-based or segmented. The reflection principle gives an advantage other SLM in terms of power handling potential[55], however DMs generally offer only a few tens of actuators across the modulation pupil and their response time is larger. As a consequence, the variety of phase modulation that DMs can reproduce is limited compared to SLMs and phase mask calculation are usually based on the first Zernike coefficients or on each actuator successive adjustment using iterative optimization algorithms[56]. An interesting study uses an SLMs to simulate the effect of changing the DM actuators size on the beam shaping quality[57]. Let us include in this family the DMD (digital micromirror device), mostly used for display application. DMD show a much thinner surface element resolution (a few micrometers) with short response time (≈ ms). However only 2 surface states available (mirror tilt angle), reducing the applications to light amplitude masking, or very particular wavefront shaping based on binary amplitude holograms (a complete review of DMD performances and applications can be found here[58].

Deformable mirrors (DM) are very well-known devices used in adaptive optics to correct for geometrical aberrations. As illustrated in Fig. 2(b)), controlling the height of a series of actuators permits to modulate the laser wavefront reflected on the device. The DMs can be membrane-based or segmented. The reflection principle gives an advantage other SLM in terms of power handling potential[55], however DMs generally offer only a few tens of actuators across the modulation pupil and their response time is larger. As a consequence, the variety of phase modulation that DMs can reproduce is limited compared to SLMs and phase mask calculation are usually based on the first Zernike coefficients or on each actuator successive adjustment using iterative optimization algorithms[56]. An interesting study uses an SLMs to simulate the effect of changing the DM actuators size on the beam shaping quality[57]. Let us include in this family the DMD (digital micromirror device), mostly used for display application. DMD show a much thinner surface element resolution (a few micrometers) with short response time (≈ ms). However only 2 surface states available (mirror tilt angle), reducing the applications to light amplitude masking, or very particular wavefront shaping based on binary amplitude holograms (a complete review of DMD performances and applications can be found here[58].

Acousto-optic deflectors (AOD) are devices whose primary goal was not related to beam shaping but to high speed deflection for multiplexing and demultiplexing optical signals and beam scanning[30]. By generating sound waves inside a crystal (e.g. TeO_2 or $PbMoO_4$) with a transducer, a periodic pattern of varying refractive index is generated and diffracts the laser beam. Thus, the phase modulation relies on the sum of periodic signals that are sent to the transducers (in x and y) where each diffraction angle contribute to the desired beam shape[59] as shown in Fig. 2(c)). Even though this technique doesn't offer the large flexibility and precision of SLMs, AODs have the advantage of much quicker response time and an inherent intensity smoothing effect due to the chromatic aberration associated with the diffraction angles, even though this also degrades the ultimate beam spot size[60].

The multi-plane light conversion (MPLC) set-up is based on the principle of spatial mode conversion through successive phase retardation masks that can be displayed with an SLM or with fabricated phase plates[61]. In the reflection scheme as depicted in Fig. 2(d)), several beam reflections on a modulation plate permit the mode conversion[62]. This technique was initially developed for the field of optical telecommunication for optical signal multiplexing and demultiplexing and is now gaining a strong interest for laser surface processing with high power lasers and ultrafast lasers[63,64]. With the advantage of high power handling thanks to the reflection scheme, the MPLC lacks dynamic straightforward reconfigurability, unless a SLM is incorporated as the modulation plate or if the modulation plate is designed to perform different shaping for different angles of the incident beam[63].

We also have to mention here the technique of general phase contrast (GPC) at the frontier of amplitude and phase modulation[65,66]. This elegant technique relies on the principle of phase contrast microscopy (PCM). There, the portion of the light beam that is diffracted by the observed phase sample is purposely put in interference with the non diffracted beam (the background light in PCM). That way, the phase contrast is turned to an intensity contrast on the microscope camera[67]. In the case

of laser beam shaping, the plane of wavefront regulation corresponds to the sample plane of the phase contrast microscope. In order to turn this phase modulation to an intensity modulation, the GPC method employs a phase contrast filter (PCF) positioned at the focal plane of a lens (Fig. 2(e))). The wavefront modulation plane is conjugated on the PCF through a lens and then the PCF is conjugated to the imaging plane. GPC achieve much lower laser intensity losses as compared to amplitude modulation[68]. This technique gives remarkable beam shaping qualities and is successfully employed in the field of optical tweezers[69]. The challenge with this technique for laser processing is related to the small disk in the focal plane of the lens. In the case of femtosecond laser with high intensity, this element can be damaged because of the laser focusing on the disk, or detrimental nonlinear propagation effect can occur and deteriorate the desired beam distribution.

Another technique that has to be discussed here is the direct laser interference patterning (DLIP) that is based on the interference of two or more coherent laser beams usually coming from the same laser source. The interference pattern constitutes a tunable intensity distribution that depends on the number of beams and their phase and angle relationship[70]. Those parameters can be tuned with diffractive optical elements (DOE) or SLMs for a higher degree of reconfigurability[71–73]. Recent efforts have been conducted towards higher processing rates including coupling with scanners and roll to roll processes[74,75].

Let us also mention the tunable acoustic gradient index of refraction lens or TAG-lens which is a is a liquid z-scanning lens operating at 0.1–1 MHz[76] permitting a very quick axial displacement of the focused laser spot enabling enhanced depth of field laser processing[77] and that has recently been used for simultaneous laser surface processing and monitoring at high speed[78]. The Table 1 summarizes the main characteristics of these phase modulation devices.

We now briefly consider the capacity of these apparatus in terms of laser power and fluence handling. From a general point of view, all the methods based on reflection can benefit from the possibility to have very high laser induced damage threshold (LIDT) reflective layer, well-adapted to the laser wavelength. This includes the DMs, DMDs, MPLC and the DLIP (unless the beam

Table 1 | Comparison of dynamic wavefront modulation techniques for ultrafast laser spatial beam shaping. See text for more details and relevant references.

Technique	Principle	Advantages	Disadvantages	Common applications
Spatial light modulators (SLM)	Liquid crystal layer controlled by electric field	High resolution (pixel size < 5 μm), 2π phase range, flexible modulation	Limited power handling, slow response time (50–100 Hz)	Ultrafast laser processing, holography, optical trapping, imaging, communications
Deformable mirrors (DM)	Actuator-driven mirror surface modulation	High power handling, non-pixelated	Limited spatial resolution (tens of actuators), slower than SLMs	Adaptive optics, aberration correction, laser beam shaping
Digital micromirror devices (DMD)	Binary tilting micromirrors	Fast response time ($\approx$ ms), high resolution	Binary phase modulation or amplitude control (energy losses)	High-speed imaging, beam steering, structured illumination
Acousto-optic deflectors (AOD)	Sound waves generating a refractive index modulation in a crystal	Fast modulation, inherent smoothing effect	Dispersion degrades focus, limited shaping flexibility	Beam scanning, multiplexing, ultrafast switching
Multi-plane light conversion (MPLC)	Successive phase masks for spatial mode conversion	High power handling, mode conversion flexibility	Limited dynamic reconfigurability unless SLM-based	Optical telecommunications, ultrafast laser processing, structured beam generation
General phase contrast (GPC)	Phase modulation converted to intensity contrast using phase contrast filtering	Low energy losses, high contrast beam shaping	Sensitive to high intensity femtosecond lasers (potential nonlinear effects)	Optical tweezers, phase imaging, structured light applications
Direct laser interference patterning (DLIP)	Interference of multiple laser beams to create structured intensity distributions	Large beam patterning	Requires phase control, limited to periodic structures	Surface structuring, micro/nanopatterning, high-rate laser processing
Tunable acoustic gradient (TAG) lens	Liquid lens modulated by acoustic waves for fast axial focus control	MHz-scale modulation, fast depth scanning	Limited lateral shaping capability	High-speed laser processing, real-time depth control, imaging

duplication is achieved with a DOE). Examples of continuous kW lasers used with such coated devices can already be found[63,79]. Considering the current efforts to optimize the interplay between the electric field distribution, refractive index and intrinsic LIDT of the dielectric layers, there is little doubt that this can be extended to high power ultrafast sources as recent developments have shown optimized multi-layer schemes with a LIDT possibly surpassing 2 J/cm^2 for ultrafast pulses[80]. LIDT appears to be more problematic for devices requiring transmission through a modulating medium as for SLMs, GPC, AOD and TAG lenses. Interestingly, the liquid crystal LIDT has been recently studied for ultrafast pulses at various repetition rates, with values ranging from 1.1 to 0.07 J/cm^2 for single shot and 1 MHz regime, respectively, showing the problematic decrease of LIDT at high repetition rates[81]. The relatively high damage threshold at single shots has triggered efforts to use gallium nitride for the transparent electrodes in the case of all-optical SLMs[82]. However, the LIDT decrease with the repetition rate has motivated SLM fabricants to propose cooled systems with sapphire cover glass for enhanced heat dissipation, allowing the use 183 W picosecond pulses at 1 MHz[83,84]. Lower LIDT should be expected for TAG lenses, AOD and GPC. Indeed, TAG lenses require a liquid (usually a silicon oil[76]), AOD are based on a crystal (TeO_2) and GPC relies on a phase filtering element at the focal plane. Thus, a reduced capacity in terms of LIDT and power handling at high repetition rates can be expected. Moreover; nonlinear propagation effects can also intervene in these media before damage, degrading the beam propagation conditions and ultimately the beam shaping quality at lower laser power. Indeed, the nonlinear refractive index of common liquid crystals like MLC2132 has been recently measured at $\approx 40\times$ that of fused silica for ultrafast pulses[85], similar values were obtained for TeO_2 crystals[86] meaning that nonlinear beam degradation before LIDT can also be envisaged at high laser powers.

Now that the main wavefront modulation techniques were accounted for, and especially the ones that have already been used for ultrafast laser processing, we focus on the calculation strategies of the modulation masks.

Calculation of the phase modulation

There are many solutions to calculate the proper spatial phase modulation, called phase mask of computer generated hologram (CGH). Usually, the phase modulation plane corresponds to the object focal plane of the focusing lens. In this case, a Fourier transform permits to mathematically relate the complex laser amplitude of this plane to the focal plane under the paraxial approximation[42] (If the phase modulation is performed in another plane, a parabolic phase term may be added to the calculation). Thus, the calculation of the proper phase modulation ϕ_M for a desired intensity distribution can be based on optimization algorithms relying on one or several Fourier transforms. Three main calculation strategies are illustrated by Fig. 3.

The most famous one is the gerchberg-saxton algorithm or iterative Fourier transform algorithm (IFTA)[87]. This deterministic algorithm performs back and forth propagation steps between the phase modulation plane and the focal intensity target plane, with the constraints of the desired focal target intensity and the original laser beam profile. Iterations go on until a phase mask permits to obtain a intensity in the focal plane close enough to the target. Many improvements have been proposed for this algorithm, such as extension to *N*-planes (in 3 dimensions)[88], dynamic adaptation of the target intensity[89,90], introduction of a 'numb' region for high fidelity shaping[91,92] and so on. It is interesting to note that many of these improvements have been triggered by the fields of optical tweezers and atomic cooling. More details on these recent advances permitting to overcome the SLMs limitations are given in Section 4.

When the intensity target is an array of distinct spots, the lens and gratings (LG) techniques are particularly adapted. The LG is based on the fact that each desired laser spot in the focal region corresponds to a given beam deflection and defocusing i.e a phase tilt and phase second order curvature. A complex sum of each contribution permits to generate the desired phase mask, without the need of any optimization step[93,94] as illustrated in Fig. 3(b). This strategy can also include position-dependent aberration correction and arbitrary intensity levels[95]. The LG strategy is similar to the generation of spot arrays with kinoforms from the optimization rotation angle algorithm[96] or with Dammann cells[97] that has also been extended in the 3D[98]. The phase modulation can also be calculated based on a ensemble of Fresnel lenses, each lens corresponding to one laser spot[36]. Researchers have also taken advantage of the Talbot effect, also enabling multispot generation in the 3 dimensions with the possibility to combine it with helical wavefront shaping[99].

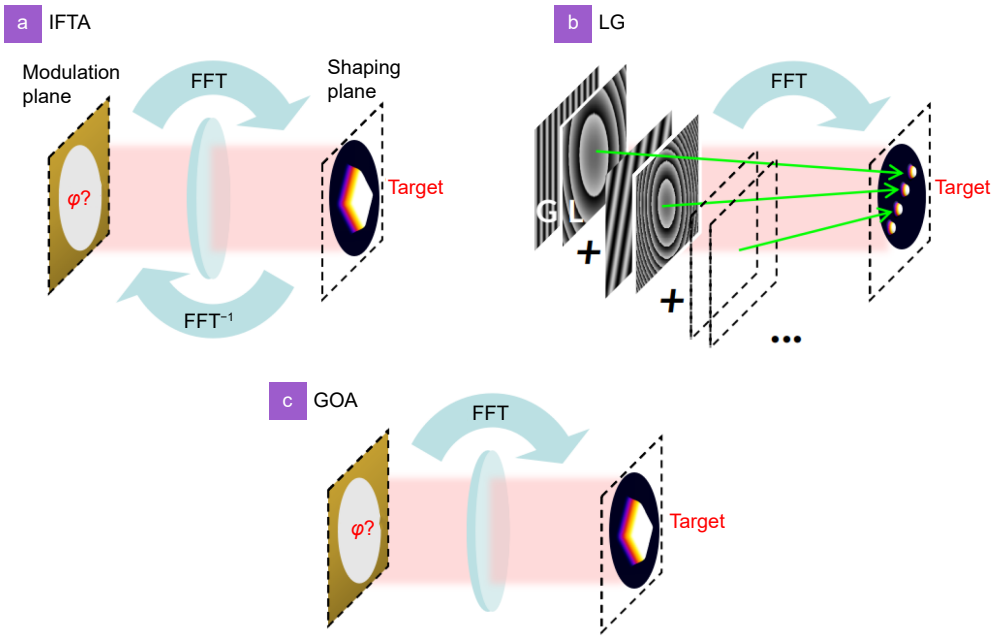

Fig. 3 | Main calculation strategies for determination of the spatial phase modulation ϕ_M. (**a**) The iterative fourier transform algorithm (IFTA) based on FFT iterations between the modulation and the shaping planes. (**b**) The lens and grating (LG) calculation relies on the complex sum of phase masks to generate arrays of laser spots in 3D. (**c**) The global optimization algorithms encompasses all the strategies that permit to 'guess' the optimal ϕ_M through stochastic optimization (simulated annealing, evolutionary algorithm etc.) or machine learning strategies (neural network etc.).

The third calculation strategy concerns global optimization algorithms (GOA). For this report, we include non-deterministic algorithms encompassing both randomized optimization algorithms and machine learning strategies. The goal is to determine the phase modulation mask $\phi_M(x,y)$ that permits to achieve a user-defined intensity distribution. The algorithm must walk a very large search space constituted by all the phase values that the phase modulator offers. The optimization can be performed numerically using e.g FFT or experimentally by measuring the laser intensity distribution. Thus, probabilistic techniques have been used for spatial beam shaping like gradient descent[100] simulated annealing[56], evolutionary algorithms[101] for spatial beam shaping but also for aberration corrections. More recently, machine learning has gained interest for laser beam shaping as discussed in Section *Advances in dynamic spatial beam shaping*.

Surface and bulk structuring with spatially shaped ultrafast laser

At the micrometric scale

In order to increase the efficiency and flexibility of the process, spatial beam shaping was rapidly included to ultrafast laser processing set-ups. The possibility offered by femtosecond pulses to produce surface and bulk structuring on multiple scale, from the nanometer to the millimeter range has motivated the researchers to make the most of all the available laser energy. Figure 4(i) illustrates various examples of surface ablation and structuring performed with the help of dynamic spatial beam shaping. An array of laser spots evidently enables parallel micromachining, thus reducing the operation cost and time. Static microlens arrays have been used quite early for parallel machining, for example to perform parallel photopolymerisation[106]. Examples of surface structuring with dynamic spatial shaping using SLMs are illustrated in Fig. 4(a–d) with the pioneering results of G Dearden team[37]. Note that the array of impacts on silicon forming the 'Liverpool' word is the result of 15 irradiation steps with different arrays of 7–9 laser spots and no sample displacement, illustrating another advantage of using spatial beam shaping for rapid processing (see Fig. 4(a)). Similar results on tempered glass were reported (see Fig. 4(b)) with an array of 9 laser spots. Interestingly, the treatment confers anti-reflection properties to the surface[102] thanks to the presence of laser induced surface structures (LIPSS) with nanometric surface modulation prone to optical effects in the visible range[11,107,108]. Noteworthy, these LIPSS patterns can be orientated with the laser polarization offering a precise control of the

related diffractive effect[109]. Thus, by generating large and uniform laser intensity distributions combined with fast scanning, rapid surface structuring at the nanometric scale is rendered possible[110,111]. Surface processing with an array of spots combined with fast scanning of the femtosecond laser beam is shown on Fig. 4(c). The structuring permits to control the surface tribological properties in a lubricated environment[112]. Another interesting example of parallel spot structuring involves the use of 15 parallel spots to generate oleophilic and hydrophobic properties on copper mesh[113] (not shown). The spot parallelization has also an interest for more rapid cutting when the processing direction follow the laser spot array orientation thus reducing the number of scans while keeping the proper fluence level[114]. Pushing the limit of the number of parallel spots to more than 1000 was demonstrated by the team of Y Hayasaki[48]. Even though numerical optimizations were put into play, it can be observed that difficulties arise to maintain a good level of homogeneity for each of the multiple laser spots (see the corresponding irradiation impact on Schott B270 glass on Fig. 4(d)).

Shaping the spot form itself can also increase processing efficiency. Contrary to the regular Gaussian distribution, top-hat intensity repartitions allow for more uniform irradiation level on the sample, thus several static optical elements are commercially available to perform the Gaussian to top-hat conversion[64,115] with an interest for a better control of the pulse overlap for surface machining[116]. By using an all-optical SLM, Sanner et al. have early demonstrated the generation and use of squared top-hat beam for ultrafast machining Fig. 4(e1) and 4(e2))[35,117]. More advanced intensity distributions such as data-matrix or Fresnel lens patterns were achieved as illustrated in Fig. 4(f) and 4(g) with SLM.

We would like to point out here two limiting factors that deteriorates the beam shaping fidelity and energetic efficiency. First, the so-called 0th order is an unwanted laser spot that gathers all the non properly addressed parts of the beam due to fill factor and other limits of the SLMs. If not taken care of, this additional spot is a detrimental waste of energy and may even badly impacts the surface as clearly visible on Fig. 4(a), 4(d) and 4(f2). Researchers have developed many strategies to overcome this issue that are discussed in Section *Advances in dynamic spatial beam shaping*. Second, the speckle effect deteriorates the homogeneity of continuous beam shapes as visible on Fig. 4(e1) and 4(f1). Usually, the phase value on the SLM (or DM/AOM) is adjusted to control the intensity distribution (i.e the amplitude) in the target

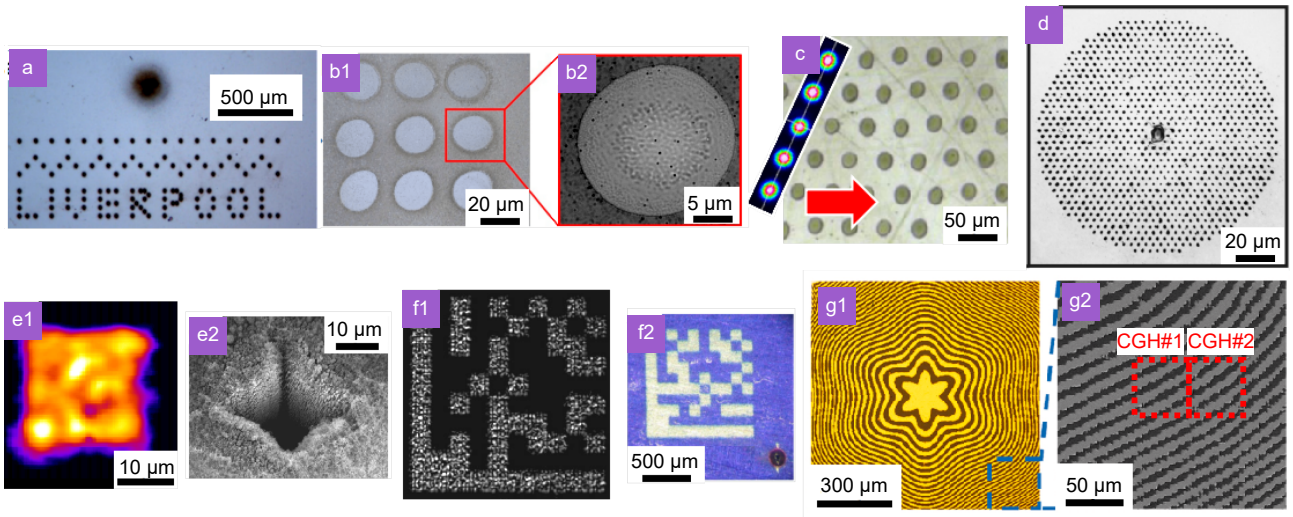

Fig. 4 | Surface structuring with dynamic wavefront shaping. (**a**) Array of impacts on silicon using 15 irradiation steps, the unwanted 0th order leaves a strong crater at the top of the array. (**b1**) Parallel structuring of tempered glass using an array of 6 laser spots with anti-reflection properties due to the LIPSS (**b2**). (**c**) Combination of multispot shaping and beam scanning for stainless steel surface processing conferring friction reduction properties. (**d**) Reaching more than 1000 laser spots in a single irradiation on glass (Schott B270), note the effect of the unwanted 0th order. (**e1**) Square top hat beam with corresponding crater on steel (**e2**). (**f1**) Shaping of arbitrary intensity distributions with the detrimental speckle effect and its marking on photoresist (**f2**) with a strong crater at the 0th order position (bottom right). (**g1**) Fresnel zone plate fabrication by successive shaped beam irradiations (**g2**) stitched together on Au film on SiO_2. Figure reproduced with permission from: (a) ref.[37], the author; (b) ref.[102], (c) ref.[103], under a Creative Commons Attribution License; (d) ref.[48], Optical Society of America; (e) ref.[35], the author; (f) ref.[104], the authors; (g) ref.[105], under a Creative Commons Attribution License.

plane. Thus, the spatial phase remains a free parameter in this target plane. This generates random phase jumps eventually leading to a superimposed random interference pattern on the laser intensity distribution[118]. The resulting speckle pattern strongly deteriorates the desired laser intensity distribution with a random pattern of darkening spots all over the beam shape. Again, several developments have been conducted to limit this effect (see Section *Advances in dynamic spatial beam shaping*). Note that for thin film ablation, polymerization or drilling, this effect may not be so problematic as the successful processing result mostly rely on overcoming a certain fluence threshold (see Fig. 4(f2, a, d, g1)). Controlling the beam shape opens the door to efficient processing of surfaces thanks to the possibility to directly 'stamp' the desired structuring map with the adequate beam shape. Using this technique, fast marking of surfaces is made possible. More advanced structures can also be achieved like this recent demonstration of super microcapacitors obtained by a single pulse laser photonic-reduction stamping based on graphene[119]. Also, advanced surface processing can be envisaged using other beam shapes like lines and rings for post-irradiation cleaning or more precise ablation compared to scanned laser spots[120,121] (not shown).

Ultrafast laser pulses have a particular interest in the case of structuring in the three dimensions inside the bulk of transparent materials[1]. Due to the non-linear aspect of the laser-matter interaction, the laser energy deposition can be achieved with a high degree of precision, reaching the micrometric and sub-micrometric levels depending on the laser focal spot size and the local modification threshold. As for surface structuring, spatial beam shaping can parallelize the process with the advantage of producing intensity distribution geometries in the 3D as illustrated by Fig. 5. In particular, 3D arrays of laser spots have been used to generate micro-modifications at multiple depths inside transparent materials[36,128] with the possibility to correct for depth related wavefront aberration[95] (see Fig. 5(a)). Another illustration of the interest of spatial beam shaping concerns the cataract surgery where an array of femtosecond laser spots can achieve the full emulsification of the crystalline lens thus reducing the need of the ultrasound handpiece for a significant increase of patient safety[9,123] (see Fig. 5(c)). Also in relation to the biomedical field, there is a general challenge to achieve efficient focusing of coherent light through opaque and/or scattering media, like skin or edematous cornea. There, dynamic phase modulation by SLMs can play a significant role, allowing for compensation of the tissue aberrations and/or scattering[129–131]. The principle here is to counterbalance the beam wavefront distortions, caused by the medias non-homogeneity[132]. Spatial light modulators can be used for microscopy and spectroscopy as well thanks to the possibility to generate multiplexed beam steering for faster sample characterization or particle trapping[133]. Other biomedical applications include the use of an array of laser spots obtained by SLM phase shaping for microsurgery, achieving multi site ablation on a Drosophila embryo[131]. Another application is related to fact that the growth cone of a developing neuron can be guided using an infrared laser beam. This intriguing phenomenon can be better controlled using a computer-driven spatial light modulator, allowing for a higher flexibility of the laser field spatial distribution[134].

Parallel structuring in glass has shown the possibility to generate photonic functions in fused silica using two processing spots[124] (see Fig. 5(d)). The direct laser writing technique inside transparent materials permits the fabrication of complex optical functions[1,15,135]. The 3D shaping potential with CGH has also been nicely illustrated using laser induced plasma in the air, thus providing 3D rendering of aerial graphics as reported by Ochiai et al.[136] (not shown). Tightly related to spatial beam shaping, aberration correction is also based on dynamic wavefront modulation that compensates for various beam deteriorations. A comprehensive review of this topic for ultrafast processing can be found here[50]. Without entering into details, let us underline that both techniques share the interest of dynamic reconfigurability offered by SLMs. In particular, when processing inside high index transparent materials, depth-dependent spherical aberrations spread out the laser intensity along the optical axis. Dynamic wavefront shaping can compensate this[125] as illustrated on Fig. 5(e). There, gyroid photonic crystals with circular dichroism properties could be fabricated in the high-index chacogenide glasses. Likewise, photonic crystals in lithium niobate were also demonstrated[126] (see Fig. 5(f)) as well as laser-induced micro-wires inside diamond[127] (see Fig. 5(g)).

Towards the nanometric scale

In order to reach the sub micrometric range for surface and bulk structuring, researchers have considered the used of non-diffractive beams. The pioneering work of

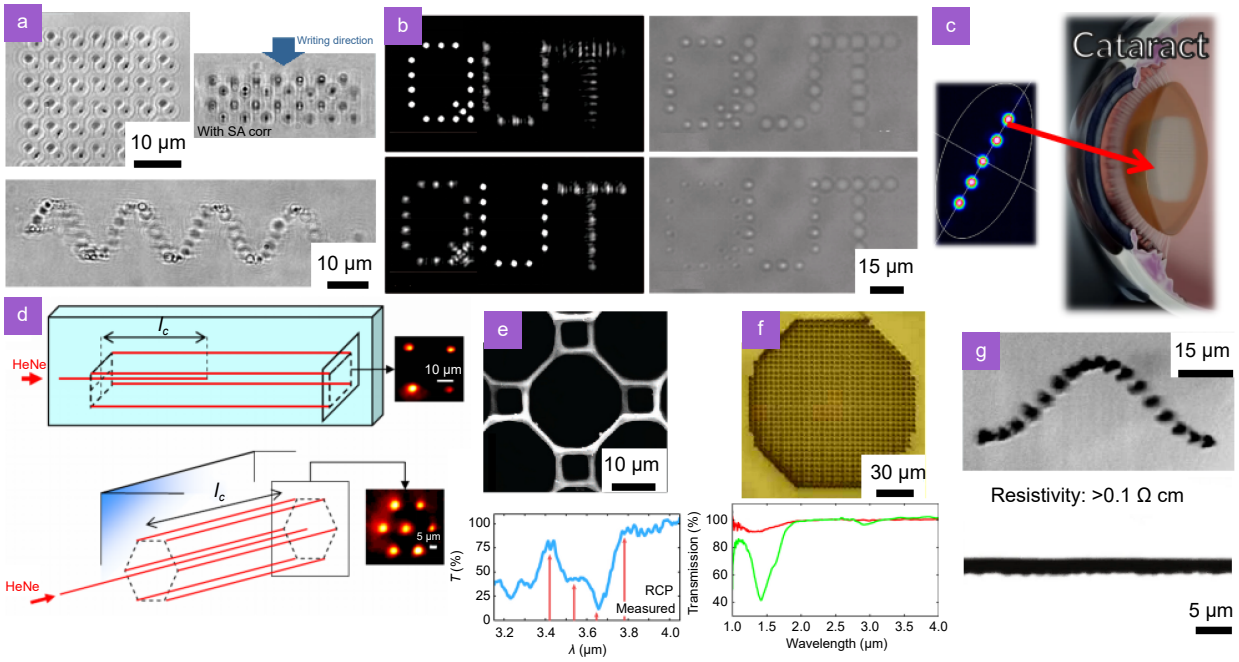

Fig. 5 | Examples of ultrafast laser bulk photoinscription with the help of spatial beam shaping. (**a**) Structuring of glass at the microscale level using 3D arrays of spots achieved in a single irradiation using LG algorithm including depth-related aberration correction. (**b**) Photoinscription in glass using the fractional Fourier transform iterative algorithm generating arrays of laser spots in multiple planes. (**c**) Photo emulsification of the crystalline lens for the cataract surgery with the help of spatial beam shaping of ultrafast laser. (**d**) Photoinscription of photonic devices inside fused silica with optical functions (here light division). (**e**) Fabrication of gyroid photonic crystals using wavefront compensation of the depth-related strong spherical aberration in chalcogenide glass generating circular dichroism (RCP: right handed circular polarization). (**f**) Photonic crystal in lithium niobate with adaptive control of the wavefront to compensate for the spherical aberrations. (**g**) Structuring of diamond in three dimension yielding conductive wires in the bulk. Figure reproduced with permission from: (a) ref.[95], the author; (b) ref.[122], the author; (c) ref.[9], the author, ref.[123], under a Creative Commons Attribution License; (d) ref.[124], Optical Society of America; (e) ref.[125], the author; (f) ref.[126], the author; (g) ref.[95,127], the author.

Courvoisier et al. has shown the interest of these Bessel beams for surface processing[144]. The experimental realization of such beam usually relies on an axiconic phase modulation that can be seen as a biprism with a cylindrical symmetry. Thus, a interference pattern is formed right after the axicon with a high intensity central lobe along a distance that mostly depends on the beam size and axicon angle. The beam formation is supported by the concentric interference of the paraxial and marginal rays, yielding a particularly long 'propagation' without diffraction and associated with remarkable self-reconstruction properties[145,146]. This results in an 10–30× confocal length increase if compared to a regular Gaussian beam of similar size. The sample surface positioning at the plane of peak intensity is therefore facilitated. Moreover, the central lobe of the bessel beam offers a tightly focused intensity easily reaching sub-micrometric dimensions. Let us be precise here that the ring pattern around the central lobe may not intervene on the structuring by properly adjusting the laser intensity so that the modification threshold remains too large for the ring patterns to permanently modify the material. Consequently, first demonstrations of structuring have shown remarkable high aspect ratio channels and stems with as little as 200 nm cross section (4 times below the laser wavelength) in fused silica and sapphire[137,138] (see Fig. 6(a)). Following this, industrial applications of such beams have risen for rapid glass cutting with low cracking[147]. Following this opportunities, reflective axicons have been developed in order to withstand high power sources with high energy pulses and wide spectrum[148]. Non diffractive and multispot shaping has also been combining to sequentially fabricate embedded spectrometers and saturable absorbers inside sulfur-based chalcogenide mid-infrared glasses[149].

Other applications taking advantage of the elongated confocal volume concern welding of transparent materials by ultrafast laser[150,151]. In that case, the gain of positioning tolerance renders the process more reliable even though several processing challenges remain, such as the

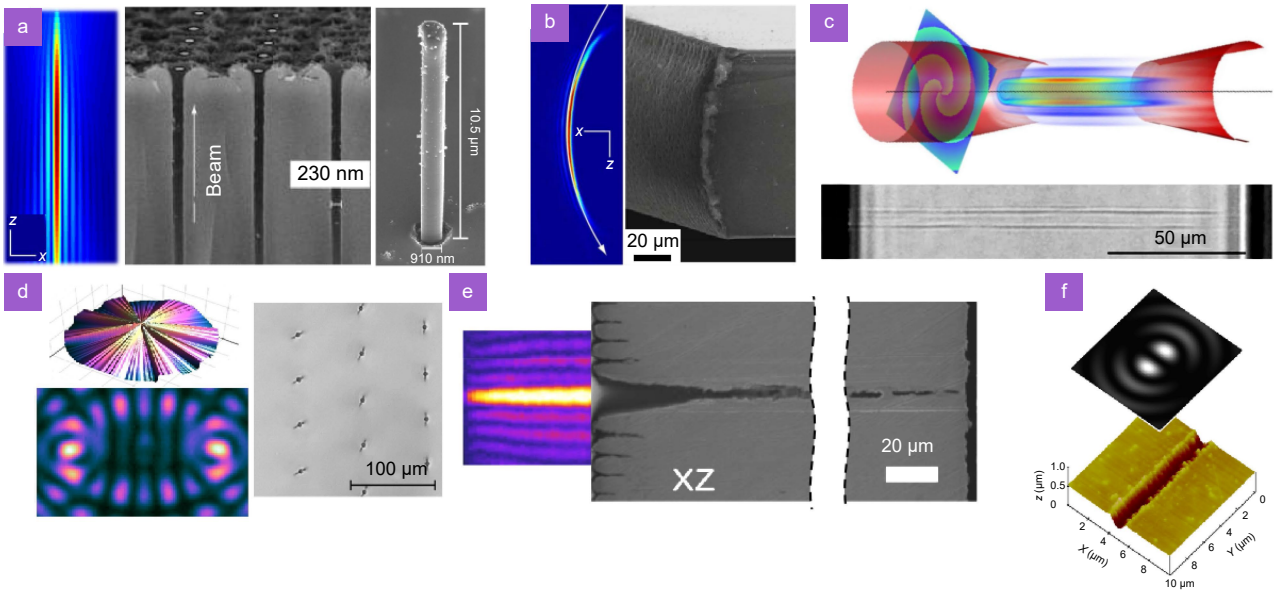

Fig. 6 | Surface and bulk structuring towards the sub micrometric scale using non-diffractive beams with the help of spatial beam shaping. (**a**) Bessel beam generation and high aspect ratio structuring of glass with single femtosecond pulses. (**b**) Turning non diffractive beam (or Airy beam) enabling curved machining of silicon. (**c**) Hollow core non-diffractive beam based on vortex phase modulation yielding tubular bulk photo inscription in a single irradiation. (**d**) Modulated axiconic phase mask forming a multiple lobes non diffractive beam permitting dynamic crack orientation control for glass cutting. (**e**) Drilling of stainless steel using non-diffractive beam with enhanced efficacy. (**f**) Machining of grooves using superimposed bessel beams associating an axicon and an SLM. Figure reproduced with permission from: (a) ref.[137], the author, ref.[138], under a Creative Commons Attribution License; (b) ref.[139], the author; (c) ref.[140], under a Creative Commons Attribution License; (d) ref.[141], SPIE; (e) ref.[142], under a Creative Commons Attribution License; (f) ref.[143], the author.

need of optical contact during irradiation[152,153] (not shown). More advanced non diffractive beams have been also demonstrated involving curved trajectories permitting round edge cutting of wafers[139] (see Fig. 6(b)). Shaping the transverse intensity distribution of non-diffractive beam has also been reported with a vortex phase modulation. In that case, a tubular bulk photo inscription in glass can be achieved in a single irradiation[140] (see Fig. 6(c)) with the possibility to generate type I and type II 3D structuring[154]. Controlling further the conical wavefront with an SLM also renders possible the inhibition or enhancement of Kerr lensing, plasma defocusing, and surface aberration effects offering means for compressing and stretching of the focal interaction volume inside transparent materials despite the strong and hard-to-bypass influence of these unstable propagation distortions[155]

Elliptical Bessel beam can also be obtained using an asymmetric phase-modulation technique with an SLM. They permit to transfer these asymmetries in the induced fields of thermo-mechanical constraints relevant for material structuring[156]. Multiple central intensity cores can also be obtained by modulating the axiconic phase mask. A better control the crack during glass cutting is then attainable in a dynamic manner along user-defined trajectories[141] (see Fig. 6(d)). Quite counter-intuitively, those beams have also shown some interest for non-transparent materials processing. Indeed, an enhanced drilling efficacy on steel when compared to equivalent fluence Gaussian beams has been reported (see Fig. 6(e)) probably due to the self-healing capacity of these beams in the presence of scattered debris[142]. Surface groove machining can also be optimized by associating axicons and SLMs. By generating superimposed bessel beams, the side ring pattern potentially producing undesired marking can be canceled[143] (see Fig. 6(f)).

Advanced nanometric structuring is also readily achievable by finely tuning the laser beam polarization with the help of spatial beam shaping. Vortex beam possessing an orbital angular momentum (OAM) have recently attracted a large attention due to their capacity to convey information within their OAM state, but also to spin micro objects or generate new imaging systems[164]. Several optical systems have been proposed to obtain such beam for ultrafast lasers[165]. This type of beams present an interest also for surface processing as illustrated

on Fig. 7(a)) where a spatial light modulator imprints an helical wavefront on the femtosecond laser beam associated with an *S*-waveplate. In that case, a particular orientation of the nanometric LIPSS can be observed on metal with a spiral geometry[157]. Dynamic change of advanced polarization states like azimuthal or radial show an particular interest when combined with surface scanning of the laser beam, producing complex LIPSS orientation reminding a soft breeze swaying over a wheat field[166,167]. Skoulas et al. have also reported on biomimetic structuring with this types of polarization usinf a *S*-waveplate only (no wavefront modulation) with the generation of complex LIPSS shapes resembling the shark's skin morphology scaled down to the sub micrometric level[168]. Hasegawa et al. have also shown the possibility to control the individual polarization of laser spots within an array of 20 lasers spots, permitting to dynamically control the LIPSS pattern[158] (see Fig. 7(b)). Interestingly, efforts have been conducted to propose compact apparatus where a single SLM simultaneously control both the holographic image and its polarization state (see Fig. 7(c)), with an interest for laser induced 5D optical storage inside glasses[169].

Going further in the structuring precision, Allegre et al. have proposed the combination of ring shaping with high numerical aperture (0.95) and polarization control to reach 10 nm surface holes on sapphire[160] (see Fig. 7(d)). It is interesting to note that such nano structuring relies on the particular nature of the laser-matter interaction at ultrafast timescales that permits to combine laser intensity distribution control with threshold effect to achieve this degree of energy localization.

Beam shaping and polarization control has recently been extended to the 3D enabling the position, polarization state and intensity control of each focal spot (see Fig. 7(e)), although not with an ultrafast beam[161]. Even if the primary applications mentioned by the authors concern optical tweezers or microscopy, the interest of this technique for ultrafast processing is evident, especially for optical data storage or the fabrication of advanced photonic components inside transparent materials. This high degree of control has also been shown for continuous beam shapes with an SLM inserted in a Sagnac interferometric set-up. In this experiment moslty dedicated to

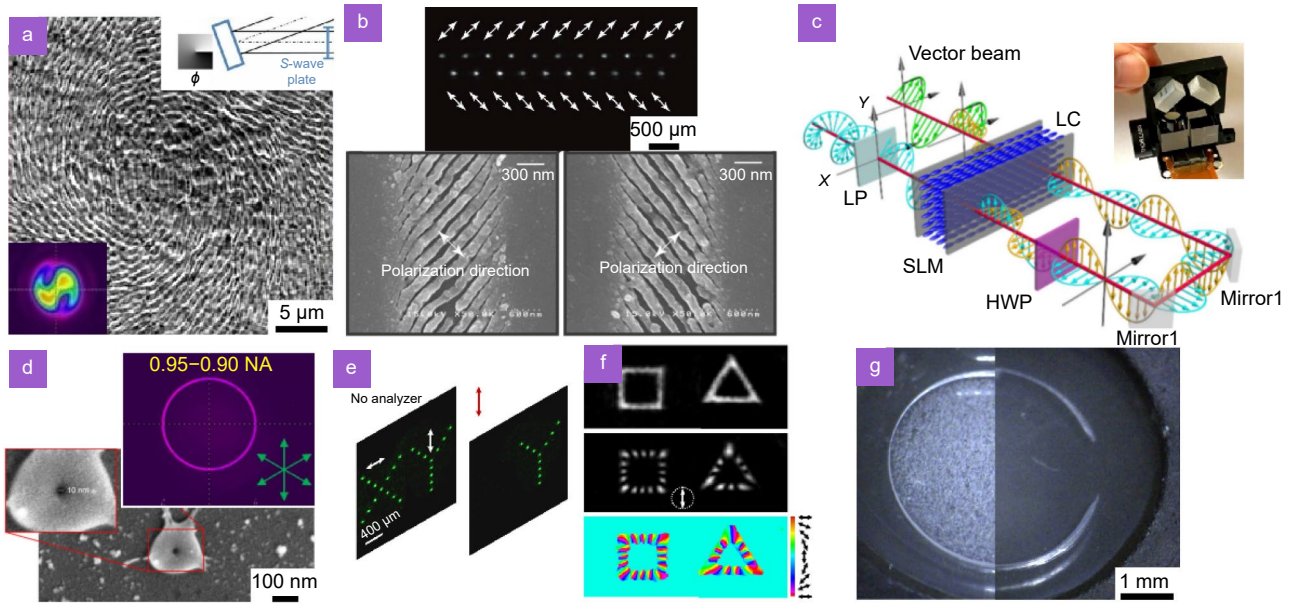

Fig. 7 | Spatial beam shaping with polarization control to achieve nanometric structuring. (**a**) Helical wavefront shaping using an SLM associated with an *S*-waveplate yielding a vortex beam generating spiral orientation of LIPSS on metal. (**b**) Array of laser spots with individual polarization control. The laser-induced surface tracks show the corresponding LIPSS orientation. (**c**) Example of integrated advanced dynamic polarization control using a single slm. (**d**) 10 nanometer surface hole on sapphire combining annular beam shaping, polarization control and high numerical aperture focusing. (**e**) Generation of spot arrays in 3D with controlled polarization (not ultrafast laser). (**f**) Arbitrary intensity distribution controlled polarization distribution (not ultrafast laser). (**g**) Cutting of cornea using vortex beam shaping (right) compared with regular Gaussian beam (left) showing a smoother and more precise cut. Figure reproduced with permission from: (a) ref.[157], the author; (b) ref.[158], the author; (c) ref.[159], (d) ref.[160], under a Creative Commons Attribution License; (e) ref.[161], the author; (f) ref.[162], the author; (g) ref.[163], under a Creative Commons Attribution License.

imaging applications, the beam polarization distribution can be tuned quasi-independently of beam intensity (see Fig. 7(f))[162]. Again, the interest of this result to increase flexibility of ultrafast laser processing seems obvious. As a remarkable combination of Fig. 6 and Fig. 7, the teams of Courvoisier and Lancry have lately demonstrated the generation of a non-diffractive ultrafast beam with a controlled state of polarization along its propagation axis. This advanced laser intensity distribution has been shown to imprint tunable chiral properties inside glass in a single irradiation[170]. We also like to point out some recent results in the ophtalmic domain with ultrafast lasers. A vortex beam obtained by helical wavefront has been used for more precise cutting of the cornea, with a lower onset of bubbles and a smoother surface finish (see Fig. 7(g))[163]. A possible explanation proposed by the authors mentions a better efficiency of the laser excitation with the ring-shaped beam due to the collagen orientation being arallel to the laser ring, contrary to the Gaussian spot, allowing for a better horizontal disruption propagation in the stroma as observed in high speed photography[171].

Following the quest of nano structuring, spatial beam shaping has also invaded additive processes like 2 photon polymerisation (2PP) and laser induced forward transfer (LIFT) that are dedicated to micro and nano fabrication to control photonic properties[179,180]. The same holds for other fields of additive fabrication involving much higher laser energy and larger processing scales like laser powder bed fusion (LPBF) and laser welding (LW), a review of the recent advances of ultrafast laser based techniques and their impact on these fields can be found here[181]. The interest of dynamic beam shaping for industrial laser processes is also discussed in ref.[182] outlining the benefit of the possibility to dynamically tune the laser energy deposition for optimized processes.

Concerning 2PP, arbitrary beam shape permits to rapidly fabricate complex structures with fine resolution in 3D by generating controlled beam shapes[172] or arrays of spots combined with beam movements[173]. This enables quick fabrication of periodic structures in 3D showing photonic band gap properties (see Fig. 8(a)) and b) respectively). Noteworthy, static microlens arrays have also been used to obtain more than 200 spots for 2PP fabrication[106]. The potential of dynamic shaping of the beam has also triggered the use of amplitude modulation device instead of wavefront modulation device. Despite the loss of energy, the quick refresh rate of digital micro mirror devices (DMD) was used to demonstrate the fabrication of 3D structures in 2PP in a continuous manner[174] (see Fig. 8(c)) or to generate an array of 10 laser spots for parallel 2PP fabrication[183]. LIFT can also benefit from these arbitrary beam shapes, by direct imprinting of the modulated laser intensity distribution[175] (see Fig. 8(d)). There also, DMD have shown an interest for the LIFT process, here in the UV range with longer pulse durations (not shown)[184]. In photo polymerization processes, the fabrication precision can be adjusted by the laser fluence level with respect to the polymerization threshold (not only with ultrafast lasers[185]). Noteworthy, this threshold can also configured by optimizing the chemistry of the light sensitive polymer[180] which can even be tuned to allow for write and erase operations[186]. Adjusting the laser fluence further also permits to achieve both local polymerization and ablation in a controlled manner during the same fabrication step[187,188]. Remarkably, the 2PP field took inspiration from the famous stimulated emission depletion microscopy (STED) technique[189,190] thanks to the possibility to finely and locally control the excitation levels. There, the gaussian excitation beam is accompanied by a ring-shaped beam that triggers depletion of the excitation levels, inhibiting locally the polymerization for fabrication resolution thinner than 100 nm (see Fig. 8(e))[176]. Even if the technique does not require a dynamic beam shaping system like an SLM to generate the ring shaped beam, it is interesting to note that recent developments imply the use of an SLM to obtain a more advanced depletion beam able to better resolve the axial origin of fluorescence photons[191]. In the same manner, the field took inspiration from the light sheet microsopy technique in order to achieve higher peak printing rates with continuous laser and optimized resins[192]. More advanced beam shaping has also been used for 2PP like helical wavefront modulation associated with coaxial beam interference that was shown to enable the fabrication of chiral microstructures depending on the beam topological charge (see Fig. 8(f))[177]. Likewise, optical vortex laser beams were used for LIFT[193] to fabricate a twisted ferrite microcrystal array by twisting and confining the sintered nanoparticles within their dark core to form chiral spinel monocrystalline dots (not shown)[194].

Concerning larger scale additive manufacturing like LPBF of LW, it is interesting to note that femtosecond laser pulses are also gaining more and more attention in these fields[181]. For example, the challenge of LPBF of high melting temperature metals like Tungsten has been

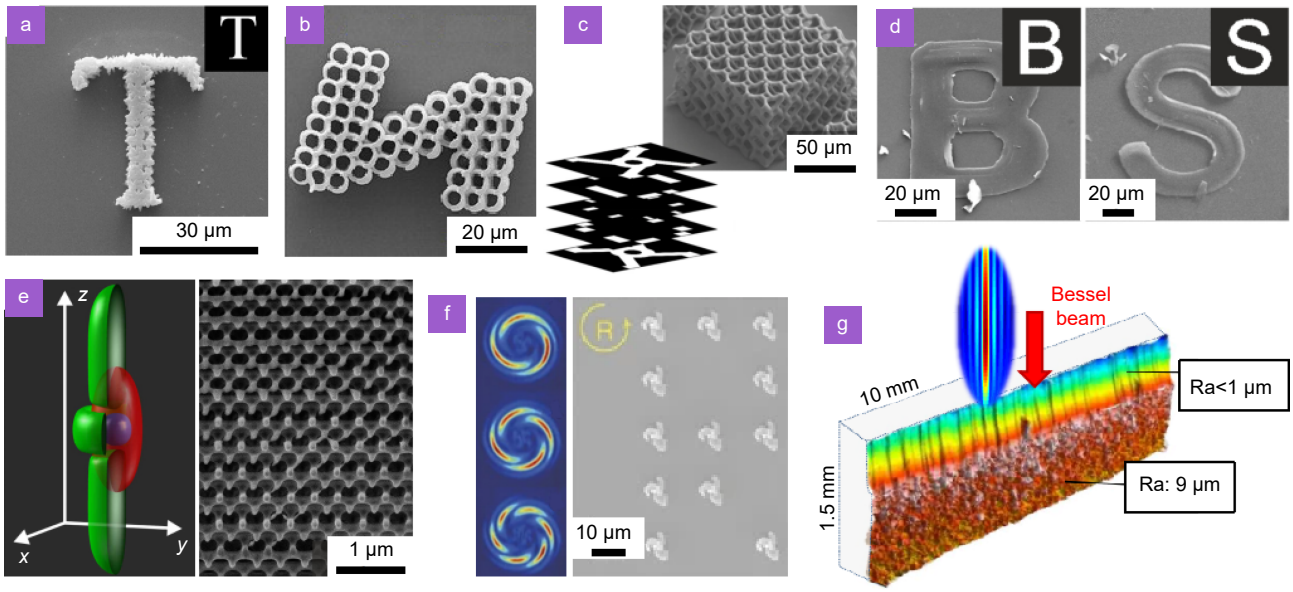

Fig. 8 | Additive fabrication using spatial beam shaping. Two photon polymerization using arbitrary beam shapes (**a**) and an array of laser spots (**b**). (**c**) Continuous projection of femtosecond pulses using digital micro-mirror device with spatio temporal focusing permits high throughput photo to polymerization. (**d**) Laser induced forward transfer of polymer on PDMS based on spatial intensity shaping using digital micro mirror device. (**e**) Stimulated emission depletion inspiring two photon polymerization combining the polymerizing beam with a ring shaped depletion beam for improved fabrication resolution. (**f**) Chiral micro structures achieved with helical phase wavefront on isotropic polymers with coaxial interference second laser beams for different topological charge. (**g**) Side wall polishing of laser powder bed fusion manufactured parts using non diffractive femtosecond beam. Figure reproduced with permission from: (a) ref.[173], the author; (b) ref.[172], the author; (c) ref.[174], under a Creative Commons Attribution License. (d) ref.[175], the author; (e) ref.[176], Optical Society of America; (f) ref.[177], (g) ref.[178], under a Creative Commons Attribution License.

recently addressed thanks to the better thermal control of the heat affected zone offered by femtosecond pulses with tunable repetition rates[195–197]. Surface roughness control and post processing of the additively manufactured parts can also be advantageously achieved by ultrafast pulses[198,199]. It can also be observed here that, as in other fields, femtosecond pulses processes are often quickly followed by spatial beam shaping developments. As an example, non-diffractive beam shaping has been proposed for side wall polishing of LPBF manufactured parts taking advantage of the longer beam confocal region (see Fig. 8(g))[178].

All these application examples, covering multiple fabrication and structuring scales, tend to show the tight link between ultrafast laser processes and dynamic spatial beam shaping. In all these cases, dynamic spatial beam shaping permits not only to push the limits in almost all matters like processing throughput or ultimate precision but also to open new doors that were previously unthought of, like curved machining with self-accelerating beams or chiral structuring with helical wavefront-shaped beams. These remarkable laboratory achievements must now face the wall of industrial-level and/or medical-level applications with the challenges of day-to-day repeatability and robustness of the process. This is where the performance of spatial beam shaping, in terms of beam intensity distribution regularity and fidelity to the target and of energy efficiency comes to play. Thus, the following section gives an overview of the numerous research efforts to ameliorate the beam shaping quality and efficiency despite the non-perfect physical beam shaping tools like SLMs and DMs.

Advances in dynamic spatial beam shaping

Towards higher beam shaping fidelity and efficiency

As the physical apparatus permitting dynamic wavefront modulation have inherent physical limitations such as limited fill factor, phase range, phase resolution (quantization) etc.; their optical response is not perfect (see a detailed review on the SLM's limitations here[205]). Concerning SLMs, the technological trends orientate towards a larger resolution with a thinner pixel pitch[49]. Despite these efforts, the aforementioned limits have a detrimental impact on the experimental laser beam shaping fidelity

to the desired target intensity distribution. Parts of the beam that are not properly modulated end up the focal spot of the focusing lens yielding the so-called stray 0th order and a superimposed random interference (speckle) pattern on the beam shape as discussed in Section *Surface and bulk structuring with spatially shaped ultrafast laser* and illustrated by Fig. 4(a, d, f2) and 4(f1). When generating arrays of laser spots for parallel machining, the stray order is usually the main challenge to overcome. A simple approach consists in adding a phase tilt to the wavefront modulation. That way, the stray 0th order can be blocked in an intermediate Fourier plane, however this drastically reduces the energy efficiency of the process[206]. Researchers have also proposed to displace axially this stray spot out of the processing plane by moving the beam shaping plane out of the lens focal plane. This can be done by superimposing a lens-type phase modulation on modulation mask[207] or by moving the coordinates of the desired spot array out of the focal plane with LG-type beam shaping strategies[208]. Another approach proposed by *M*. Booth teams takes advantage of the LG algorithm. The principle is to purposely add the 0th spot in the phase mask calculation with an experimentally adjusted piston phase at the position of the stray order in order to produce a destructive interference, allowing for more controlled processing inside transparent materials (see Fig. 5(a)) where no stray damage is visible within the 3D array of impacts)[95]. Another method has been also described by Rontizi and al.[209]. With a preliminary characterization of the SLM, the pixel cross talk effect can be counteracted permitting a reduction of 96% of the 0th order.

One of the most evident physical limitations is related to the limited resolution of the wavefront modulator. Because of the finite spatial dimension of pixels of SLMs (or actuators for DMs), the device acts as a low-pass filter with respect to the spatial frequencies of the desired phase modulation pattern. To a certain extent, this problem can be compensated by enhancing the part of higher frequencies of the phase mask permitting to obtain a more homogeneous array of laser spots (see Fig. 9(a))[200]. Interestingly, the use of an SLM in combination with microlens arrays (MLA) was recently presented[210]. The technique allows to control the individual laser spot intensities orders by varying the absolute phase with the SLM with a strong interest for coherent beam combining.

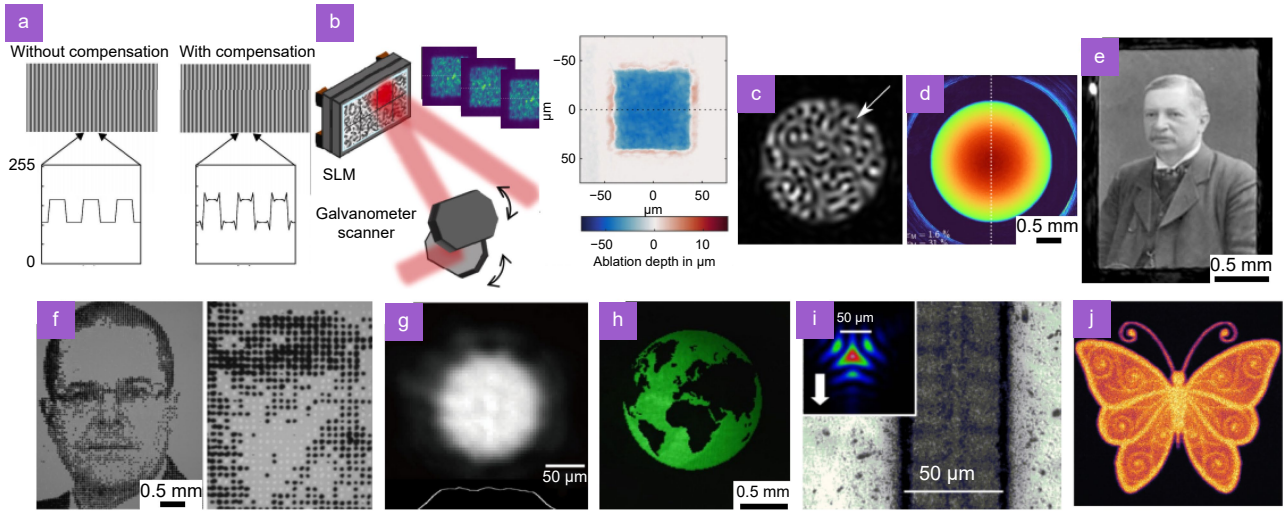

Fig. 9 | Examples of recently developed to improve the fidelity and/or efficacy of spatial beam shaping. (**a**) Compensating the limited spatial resolution of SLM by using spatial frequency filtering of the phase modulation. (**b**) Averaging the detrimental speckle effect by addressing different phase masks on the SLM for uniform multi-pulse ablation. (**c**) Incorporating Vortex elimination during the phase modulation calculation step. (**d**, **e**) High fidelity intensity distribution shaping in the region of interest with the compromise of energy losses for atom trapping. (**f**) Parallel surface structuring using multi-spot arrays with individually controlled spot intensity based on an optical feedback of the experimental intensity distribution. (**g**) Smooth top hat generation using optical feedback to adjust the intensity pattern in the iterative Fourier transform algorithm. (**h**) Arbitrary intensity distribution using the GPC technique. (**i**) Groove machining with controlled intensity distribution using Zernike polynomials optimization. (**j**) Spatial beam shaping based on diffractive optical neural network. Figure reproduced with permission from: (a) ref.[200], the author; (b) ref.[201], under a Creative Commons Attribution License; (c) ref.[118], Optical Society of America; (d) ref.[202], (e) ref.[92], under a Creative Commons Attribution License; (f) ref.[90,92], Optical Society of America; (g) ref.[203], the author; (h) ref.[65,68], the author; (i) ref.[204], Optical Society of America; (j) ref.[226], under Optica Open Access Publishing Agreement.

Another study has identified phase modulations that an SLM with limited resolution and phase depth can still correctly reproduce[211].

Concerning the detrimental speckle effect which is more related to continuous intensity distributions like round, square top-hats or arbitrary shapes, researchers have taken advantage of its random character to correct for its effect. By applying a series of similar phase masks with slight differences (e.g adding a phase piston), similar intensity distributions are obtained with a distinct speckle pattern. By displaying these various phase masks during surface ablation, an averaging effect occurs in the machining region yielding much more uniform ablation profile[104]. The technique adds a time constraint on the machining pace directly related to the relatively low refresh rate of SLMs ($\approx$ 50 Hz) and the number of necessary irradiation overlaps. However this delay can be reduced by scanning the beam on a the surface of a single SLM displaying this collection of phase masks (see Fig. 9(b))[201,212]. This solution is still limited to multi-pulse process. Note that simple beam scanning also yields an averaging effect[213]. However this confines ultrafast processes to multi-pulse machining.

Looking at solution without pulse averaging, developments around the phase calculation have also been conducted especially on the IFTA thanks to the possibility to add all sorts of constraints to this algorithm. One of them implies the elimination of vortex-like phase micropatterns within the phase modulation map directly generating zeroes of intensity in the beam shaping plane (see Fig. 9(c))[118]. Going further in this type of constraints, the IFTA was completed with the mixed-region-amplitude-freedom (MRAF) strategy by researchers mostly dedicated to atom trapping, where the fidelity of the shaped intensity distribution is much more important than the energy efficiency. In short, the MRAF consists in allowing the IFTA to freely redirect laser intensity out of a region of interest to avoid the phase vortices mentioned above. By doing so, a significant amount of the laser energy is then wasted in the numb area and in the stray 0th order (more than 50%)[91]. However, the degree of beam shaping control is remarkable (see Fig. 9(d, e))[92,202]. A similar idea was also proposed by adding the constraint of an uniform phase within the region of interest in the image plane during the IFTA[214]. Further control of the beam involves both amplitude and phase control with the use of two modulators, or two portions of a single SLM surface permitting a significant reduction of the speckle effect as well as 0th order suppression, however the amplitude modulation implies a certain energy loss[215]. Beam transformation from gaussian to high quality top-hat intensity distributions has also been shown using a phase-only SLM to achieve full amplitude and phase control with physical filtering of the 0th order[110].

Another type of strategy to circumvent the SLMs limitations, as well as some of the experimental imperfections (aberrations, misalignements etc.) is based on real-time characterization of the targeted intensity distribution, thus providing an experimental feedback. The technique is tightly linked to the IFTA algorithm as the target intensity, instead of being constant during the IFTA optimization, is gradually adapted to include and compensate for the differences between the used defined target and the experimental intensity profile. A self-explanatory example is the generation of an array of uniform spots. For the first IFTA run, the numerical intensity target is the desired array of homogeneous spots. By capturing the experimental array (which is very likely to be not homogeneous) a new weighed target is defined to compensate for the array inhomogeneities, with higher spot intensities where the the experimental ones were too weak and lower spot intensities for too high spots. This new target feeds a novel IFTA iteration. This weighed IFTA (WIFTA) process is repeated until a sufficient degree of experimental precision is reached. The technique has been used to generate arrays of laser spots with precisely controlled intensity for surface marking (see Fig. 9(f))[90], structuring of highly regular dimples on steel[103] and reach more than 1300 parallel laser spots with a optimized spot homogeneity[48]. Noteworthy, spot array homogenization can also be factorized by identifying and removing undesired phase rotations during the IFTA[216]. The WIFTA strategy based on optical feedback has also recently been used to produce smooth top-hat beams with no speckle effect neither 0th order (see Fig. 9(g))[203].

Although not being easily adaptable for ultrafast pulses as discussed in Section *Dynamic spatial beam shaping apparatus*, the high quality of intensity distribution obtained with the GPC technique has to be mentioned here (see Fig. 9(h))[68]. The technique is elegantly based on phase contrast microscopy and thus doesn't require any phase mask calculations. However, the indispensable phase filtering at the focal position of a Fourier plane is easily affected even by slight non linear propagation effects associated with femtosecond pulses, degrading the beam shaping quality (not shown). Nevertheless, recent

improvements of the technique were achieved by combining it with an additional SLM to achieve multi-plane GPC in the 3D[217]. A similar technique was used to produce highly uniform squared top hat beam, by using a superimposed diagonal phase grating for easier filtering in the intermediate Fourier plane[218].

As the main challenges related to high fidelity beam shaping are related to the limitations of the phase modulators, we recently proposed a phase mask calculation that can take into account the light modulator limits from the start, contrary to the usual IFTA or LG approaches. The key idea is to run the phase modulation calculation on a set of Zernike polynomials that the modulator can correctly reproduce. The technique is valid for SLMs, DMs and more generally any phase only modulator whose optical response can be well-characterized this way. Groove machining with a controlled ablation profile distribution could be achieved using the technique (see Fig. 9(i))[204].

Let us also mention the current strong push of machine learning strategies. Several studies compare its performance with IFTA[219] or associating it with IFTA methods[220]. An interesting review of the latest developments can be found here[221]. Usually based on neural networks, a collection of phase masks and propagated intensity distributions constitutes the training dataset permitting a faster determination of the proper phase mask generating the desired intensity distribution than IFTA methods (once the training is correctly completed)[222,223]. However, several studies outline the fact that the beam shaping quality using CNN does not surpass IFTA-based optimizations for 2D beam shaping[219] as well as multi-plane beam shaping[223]. Machine learning has also been used to correct for optical aberration in the case of muliple spot laser beam surface machining using adaptive optic convolutional neural network on Zernike polynomials[224]. Let us precise that this type of dynamic aberration correction during parallel machining was already achieved without machine learning[50,225]. Following the machine learning trend, SLMs were also employed as diffractive neural network with the scope to define efficient beam shaping modulations for better performance against misalignments or when using binary DOEs[226] but also with a lower stray 0^{th} order[227]. Although not directly related to beam shaping, let us mention here the current widespread trend to use machine learning and optimizations strategies with rapid monitoring of the processed area[228]. Examples of using such techniques for improved ablation efficiencies or LIPSS generation are flourishing in the literature[229–231], even if this concept of self-learning ultrafast processes with in-situ feedback loop was demonstrated much earlier for transparent material machining[232,101]. There is no doubt that such optimization strategies will increasingly involve advanced spatial beam shaping in the near future.

Several efforts were also conducted on the SLM architecture itself in order to obtain better performance for dedicated beam shapes. For example a transmitting SLM based on LC with electrodes having a sector geometry has been proposed, allowing for helical wavefront shaping and vortex beam generation[233]. In the same trend, a polymerizable nematic liquid crystal was used as the active wavefront medium in a custom SLM. By achieving local polymerization by 2PP, the authors could imprint in the LC layer an arbitrary static phase modulation that can be activated and deactivated with the application and removal of an external applied voltage. The technique was shown to be efficient for aberration correction[234] or multi-spot pattern generation based on Dammann grating[235]. The quest of faster response time has also led to several studies. In is known that increasing the temperature of the LC permits to decrease the viscosity, offering a higher reorientation speed. However, this degrades the phase modulation stability, augmenting the flickering effect[236]. Thus, ferroelectric LC layers were employed to reach faster response time, up to 6.3 kHz for binary phase modulation[54,237,238]. Let us briefly mention here that in many laser processing situations, the need for rapid beam shape change is not mandatory. In many cases, surface or volume structuring/cutting is conducted with a constant phase modulation throughout the laser processing (see for example[103,200,144]. If this remark pleads in favor of static phase modulation apparatus (DOEs, MPLC etc.), it is worth noting that the possibility to dynamically change the phase modulation, even at a limited rate, significantly increases the processing flexibility by e.g addressing depth-related aberrations[50,125] changing the marking or ablation target shape[90,105] or correct for beam distortions[203].

More recently, the question of power handling has become a central issue because of the remarkable advances of the commercially ultrafast laser sources in terms of available power[3,4] and the growing demand of ultrafast laser processing with the use of spatial beam shaping (see various application examples in these references[103,123,141,239]). Thus, a technique permitting to

optimize the beam size on dual-SLMs set-up in order to decrease the impinging laser fluence was proposed[240]. It also has been shown that the temperature-dependence of the LC layer phase modulation can be taken into account for stable multispot generation[241]. Investigations of the SLMs behavior at high laser powers (around 200 W) have been reported[53,242]. The heat accumulation on the SLMs implies a decrease of the available modulation phase range, yielding a degradation of the beam shaping quality with more wasted energy in the stray 0th order[53]. A study of optically-induced thermal non-linear effect in a nematic liquid-crystal has been done using an optically addressed SLM through weak light-absorption of the photoconductive material, showing beam distortion such as spatial self-phase modulation[243]. Noteworthy, the same research team has proposed an interesting SLM architecture taking advantage of the thermo-optical effect for large spectral bandwitdh with a large modulation dynamic range, the so-called Thermo-Optically-Addressed Spatial Light Modulator (TOA-SLM)[244]. By impinging a single gold layer with a modulation beam, a local temperature gradient is generated, affecting the attached LC layer yielding a corresponding phase modulation on the readout laser beam. There also, machine learning was used, in order to generate prescribed low-order spatial phase modulations with a little amount of experimental data[245].

Research involving the use of other devices than SLMs has also been conducted. For example, beam shaping using AOD was studied to achieve flat top intensity distributions (see[60] and references therein). Turning beams similar to those obtained with SLMs (see Fig. 6(b)) were also demonstrated by using an acoustooptic cell with a cubic phase transmittance, as well as other interesting accelerated beams[246,247]. Developments around the MPLC device, particularly interesting thanks to its inherent high power handling capability, have also involved the use of machine learning to find optimal triangular beam shapes for Fresnel lens fabrication[248]. The so-called grating light valves (GLV) are also gaining attention for laser processing thanks to their very high refreshing rate (more than 300 kHz)[249], even though the optical configuration is based on a one-dimensional SLM and imaging which renders the optical set-up more complex. Interestingly, researchers have also combined DOEs with AOD to obtain rapid reconfigurability of spatial beam shaping thanks to the quick response time of AODs[250]. Amplitude modulation was also studied in combination with phase modulation using two SLMs, the first one enabling beam shape control by imaging[44] and the second one multiplying the number of shaped spots for parallel processing through phase modulation[251]. Inspiration for ultrafast processes with advanced beam shaping can also be taken from the field of LPBF where various controlled beam shapes (top-hat, ring, elliptical, Bessel) have a strong impact on the melting pool dynamics and the final structural properties of the fabricated parts[252].

A promising research direction for dynamic beam shaping concerns tunable meta surfaces[253]. In these 2D devices, the properties of subwavelength elements are controlled on order to modulate the impinging light phase, amplitude and/or polarization. With a very high potential in terms of integration to optoelectronic devices, several schemes have been proposed achieving beam steering[254] (related to the key application of LIDAR), beam focusing[255] and advanced holography[256]. Noteworthy, ultrafast lasers can play a key role in the fabrication fo these surfaces[257] thanks to the possibility to highly localize the laser structuring with recent results involving SLM-based laser beam shaping for the processing[258]. Several materials of interest are under investigation (e.g phase-change materials such as Ge-Sb-Te (GST), noble metals whose optical properties can be switched through hydrogenation and subsequent dehydrogenation, liquid crystals, transparent conductive oxides, graphene etc.)[253]. Applications for ultrafast laser processing with meta surfaces based spatial beam control are now at reach, also facing the challenges of efficiency, power handling and shaping quality.

In short, research efforts around ultrafast laser processing using dynamic spatial beam shaping are mainly addressing the issues of beam shaping fidelity and efficiency, trying to counteract the detrimental effects of the physical optical response of light modulators. The increase of available power handling pushes the work around efficient spot parallelization, controlled beam forming and reflective solutions able to withstand both high average power and peak intensities. Machine learning has already gained a strong interest in the field thanks to its quick phase mask determination and to its adaptability to various laser processes especially when a rapid and/or in-situ feedback is available. The near-future trends comprehend technological developments for high power laser handling along with machine learning strategies to increase the beam shaping speed and quality. In the following, we strive to foresee some future and

more fundamental research trends based on a careful consideration of the spatio-temporal effects associated with spatial beam manipulation.

Perspectives offered by spatio-temporal

As often in science, something that is at first considered as a problem to solve is likely to become an interesting subject to explore, e.g the ultraviolet catastrophe. This also stands true for ultrafast laser processes and temporal effects associated with spatial beam shaping in general. Contrary to the quasi-monochromatic assumption taken at the beginning of this paper, ultrafast pulses carry a non negligible spectral content with consequences on their spatio-temporal characteristics during the beam propagation depending on the optical elements met on the beam path. We will not discuss here the details of temporal pulse shaping and its interest for ultrafast laser processing as this subject is beyond the scope of the review[265–269]. However, a closer look at the specificity of ultrafast pulses when spatial beam shaping is employed reveals situations where the pulse temporal excitation during processing is greatly affected, even for simple beam shaping elements. Considering the spatio-temporal characteristics of femtosecond pulses leads to the notion of pulse front. This quantity corresponds to the spatial surface that comprehends the intensity peak of the pulsed laser beam. In vacuum, the phase and the pulse fronts are identical as they travel respectively at the phase and group velocity that are also equal. However, in a isotropic and dispersive media like glass, their speed differs due to the variation of refractive index with respect to the wavelength. In this simple case, a delay takes place between the pulse front and the phase front while they keep an identical spatial distribution. The situation becomes more complex when a beam passes through an non-flat optical element constituted of a dispersive material, like a fused silica lens. Z. Bor has conducted several pioneering theoretical and experimental studies, revealing the effect of pulse front distortion occurring when using lenses and telescopes[270,271]. For example, the use of a non-treated fused silica lens for ultrafast beam focusing can turn a spectral bandwidth-limited 100 fs pulse into a more than a picosecond excitation at the focal point, primarily due to the pulse front distortion, the group velocity dispersion being of much weaker importance[259]. The spatio-temporal cartography of corresponding pulse front distortion before and after the focal point is depicted on Fig. 10(a)). The marginal part of the pulse front-encountering less glass thickness-reaches the focal point earlier than the paraxial part, yielding a drastic increase of the local excitation. Experimentally, the team was able to precisely quantify this type of pulse front distortions using a Michelson-type interferometric set-up[270]. Naturally, the very first reaction of any well-minded scientist is to find ways to avoid this alteration of the laser excitation. Indeed, it can simply be achieved by using achromat lenses and more generally by avoiding any chromatic aberrations on the beam path. However, the pulse front can also be considered as an additional control knob for ultrafast laser processing. One of the first interesting results that was reported being related to the pulse front control of ultrafast laser pulses is the so-called quill-writing effect. The team of P. Kazansky has thus reported the intriguing phenomenon of non-reciprocal photo-writing using ultrafast pulses depending on an onset of spatial chirp and pulse front tilt (see Fig. 10(b))[260]. This type of pulse front distortion coupled with spatial chirp is often met at the output of amplified ultrafast sources because of the the recompression stage geometry[272]. The results reported by P. Kazansky can be seen as the first developments around advanced processing using pulse front control[273]. The possibility to control not only the wavefront but also the pulse front has opened a new avenue for dynamic control of the region of highest laser intensity within the focal volume. As well-explained in ref.[263], considering a laser beam with a linear spatial chirp passing through a lens with chromatic aberrations yields a space and time-varying focal spot. This is because the bluer part of the beam is focused earlier than the redder part. This can be extended to more complex pulse front shapes. M. Booth and colleagues have proposed an interesting setup combining SLM and DM to control both the phase and the pulse fronts[261] see Fig. 10(c)). This permits to control the focal intensity velocity, yielding the so-called flying focus, with arbitrary controlled subluminal or superluminal speeds (see Fig. 10(d))[262]. Numerical simulations permit to precisely anticipate the spatiotemporal behavior of the laser pulse around the focus in z versus time diagrams like the one depicted on Fig. 10(e)) with the possibility to generate several accelerating and decelerating steps of the local excitation peak[263]. This advanced level of excitation control might constitute a decisive advance in the field of ultrafast processing, especially of in-volume processing of materials that are transparent to the laser wavelength. Looking closer, the possibility to drive an excitation

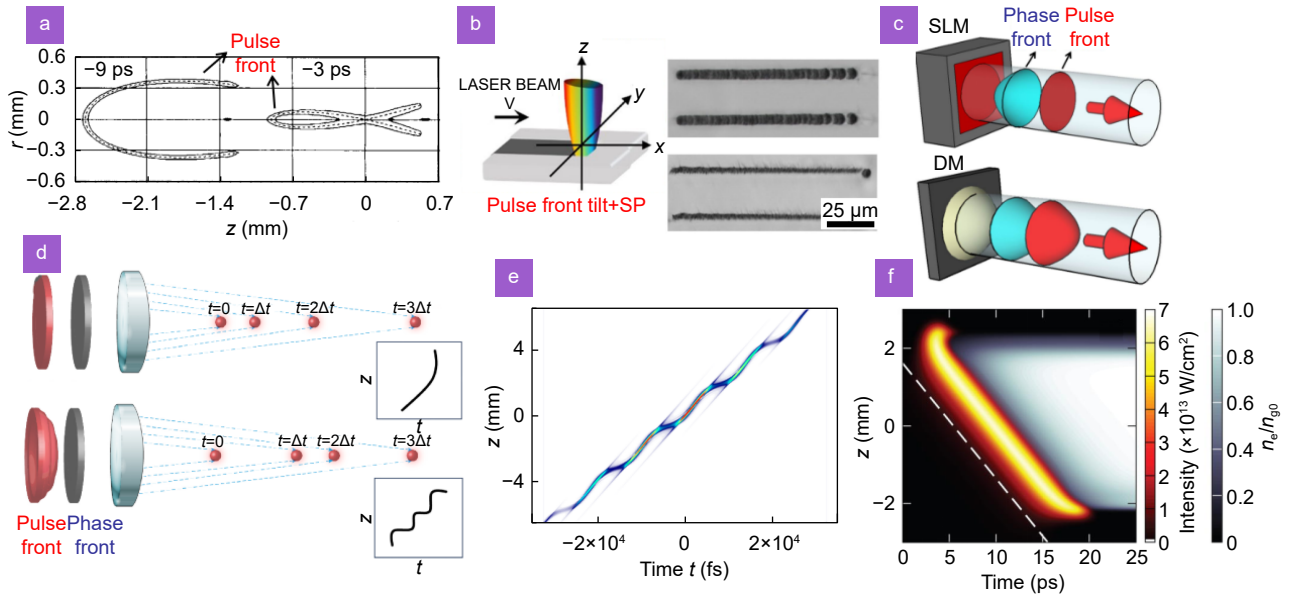

Fig. 10 | Future research trends taking advantage of the temporal effects associated with spatial shaping. (**a**) Illustration of the pulse front distortion around the focal point implying complex consequences on the spatial and temporal properties of the local excitation. (**b**) Pulse front tilt and spatial chirp involving non reciprocal photo inscription on glasses. (**c**) Concepts for pulse front and wavefront modulation based on an SLM and a DM. (**d**) Controlling the velocity of the intensity focal point in the focal region along *z* by tuning the pulse and phase fronts. (**e**) Simulation of a controlled intensity trajectory with accelerating and decelerating steps. (**f**) Overcoming ionization induced refraction by controlling the flying focus speed. Figure reproduced with permission from: (a) ref.[259], Springer Nature; (b) ref.[260], under a Creative Commons Attribution License; (c) ref.[261], the author; (d) ref.[262], under the Optica Open Access Publishing Agreement; (e) ref.[263], the author; (f) ref.[264], the author.

region spatially at superluminal speeds offer a much higher degree of control (see the visualizations in ref.[263]), possibly overcoming light delocalization effects like plasma shielding due to the material transient response that are detrimental for precise bulk processing. A well-known example of this challenge concerns precise bulk microstructuring inside crystalline silicon (*c*-Si) using ultrafast pulses. Remarkable efforts have been made to bypass the very high degree of light delocalization of this material by using longer pulses (in the picosecond and nanosecond regime), femtosecond-pulse trains, and surface-seeded bulk modifications[274]. Recently, Froula et al. have experimentally reported the generation of a flying focus quicker the ionization-induced refraction in air (see Fig. 10(f))[264]. It can be anticipated that similar developments take place for highly localized bulk processing of c-Si or other transparent materials.

Conclusions

In conclusion, the use of ultrafast lasers for surface and bulk processing has gained a strong interest, due to their capacity to achieve high precision in ablation, cutting, and structuring processes with relatively low thermal side effects. Dynamic spatial beam shaping, particularly using spatial light modulators, emerges as a promising solution to efficiently use the growing laser power or commercially available sources. This technique gains particular relevance with the emergence of Ytterbium-based laser sources, distinguished by their much higher power and repetition rates when compared to conventional Ti:Sa lasers.

Several factors underscore the critical role of spatial beam shaping in the realm of ultrafast laser processing. Spatial beam shaping permits the sculpting of the laser intensity distribution in a quasi-arbitrary fashion, increasing the processing precision by spatially tailoring fluence levels. This is of great benefit for applications requiring micrometric spatial structuring resolution, especially when the interaction involves a rigorous control with respect to structuring threshold (LIPSS formation, 2PP, ablation etc.). Precision alone is not enough for game changing processes. Efficiency also stands as key advantage offered by the technique. By controlling the beam shape, the available laser energy can be distributed more effectively, facilitating parallel processing and enabling the creation of customized beam shapes that can be designed for specific applications, non diffractive beams being a very illustrative example in quest for

submicrometric cutting/ablation. Thirdly, flexibility is a noteworthy benefit. Dynamic spatial beam shaping offers the agility to dynamically adjust the laser beam shape during processing, adapting to depth-related aberrations, evolving target shapes, or rectifying beam distortions on the optical set-up.

It is however essential to acknowledge the inherent limitations associated with dynamic spatial beam shaping, primarily stemming from the physical apparatus employed for wavefront modulation. Spatial light modulators (SLMs), while extensively utilized for dynamic phase retardation, encounter constraints in both power handling and response time. These devices are also susceptible to issues such as limited fill factor and phase resolution involving undesirable effects, including the emergence of stray 0^{th} order beams and the formation of speckle patterns. Deformable mirrors (DMs), while affording superior power handling capabilities, grapple with restricted spatial resolution and protracted response times in contrast to SLMs. Alternative techniques, including general phase contrast (GPC), present minimal energy losses but exhibit heightened sensitivity to high-intensity femtosecond lasers. Multi-plane light conversion (MPLC) as well as direct laser interference patterning (DLIP) permit the creation of tunable intensity distributions but present constrained dynamic reconfigurability.

Recent efforts in dynamic spatial beam shaping aim at surmounting these limitations and augmenting beam shaping fidelity and efficiency. These advancements encompass aberration correction, wherein dynamic wavefront shaping compensates for depth-dependent spherical aberrations, particularly when conducting processing inside transparent materials. Furthermore, optimization algorithms, including iterative techniques such as the IFTA and machine learning strategies, are deployed to obtain phase modulation masks less prone to the formation of 0^{th} order and speckle patterns, thus realizing desired intensity distributions. Real-time characterization of the targeted intensity distribution has been used as experimental feedback, to rectify SLM limitations and experimental imperfections. Novel techniques, like GPC and Zernike polynomial optimization, offer alternative methodologies for attaining high-fidelity beam shaping. Tunable meta surfaces hold considerable promise for dynamic beam shaping, characterized by elevated integration potential.

Power handling constitutes a critical consideration in the context of dynamic spatial beam shaping. Various devices and techniques exhibit disparate capacities for managing laser power and fluence. Methods based on reflection, such as those employing DMs, DMDs, and MPLC, can benefit from the possibility to have high laser-induced damage threshold (LIDT) reflective layers. Conversely, devices necessitating transmission through a modulating medium, like SLMs, GPC, AOD, and TAG lenses, may confront challenges pertaining to LIDT especially at high repetition rates.

Looking ahead, research groups are progressively exploring the spatio-temporal effects intertwined with spatial beam shaping. Controlling the pulse front, in conjunction with the wavefront, unlocks novel possibilities for ultrafast laser processing. For instance, the flying focus technique, which enables a certina control of the focal intensity velocity, has the potential to circumvent light delocalization effects and increase bulk microstructuring precision.

The successful transfer of dynamic spatial beam shaping from laboratory experimentation to robust industrial and medical applications relies on carefully addressing the challenges of repeatability, robustness, and energy efficiency. Future trajectories include technological innovations related to high-power laser handling, ameliorated optical performances (resolution, fill factor), deployment of efficient algorithmic strategies for refined beam shaping, tunable meta surfaces and control of spatio-temporal effects.

References

1. Itoh K, Watanabe W, Nolte S et al. Ultrafast processes for bulk modification of transparent materials. *MRS Bull* **31**, 620–625 (2006).
2. Vorobyev AY, Guo CL. Direct femtosecond laser surface nano/microstructuring and its applications. *Laser Photonics Rev* **7**, 385–407 (2013).
3. Sibbett W, Lagatsky AA, Brown CTA. The development and application of femtosecond laser systems. *Opt Express* **20**, 6989–7001 (2012).
4. Brauch U, Röcker C, Graf T et al. High-power, high-brightness solid-state laser architectures and their characteristics. *Appl Phys B* **128**, 58 (2022).
5. Pouysegur J, Gruson V, Ferachou D et al. Kilowatt femtosecond lasers for high productivity. In *Proceedings of the Conference on Lasers and Electro-Optics* ATh4P. 2 (Optica Publishing Group, 2021). http://doi.org/10.1364/CLEO_AT.2021.ATh4P.2.
6. Dominik J, Scharun M, Dannecker B et al. Multi-kilowatt ultrafast laser with thin-disk technology. In *Proceedings of the Laser Congress 2021* AM2A. 6 (Optica Publishing Group, 2021). http://doi.org/10.1364/ASSL.2021.AM2A.6.

7. Buldt J, Stark H, Müeller M et al. Broadband ytterbium fiber CPA-system delivering 120fs, 10 mJ pulses at 1 kW average power. In *Proceedings of 2021 Conference on Lasers and Electro-Optics Europe and European Quantum Electronics Conference* 61 (Optica Publishing Group, 2021). http://doi.org/10.1109/CLEO/Europe-EQEC52157.2021.9542142.
8. Juhasz T, Loesel FH, Kurtz RM et al. Corneal refractive surgery with femtosecond lasers. *IEEE J Sel Top Quantum Electron* **5**, 902–910 (1999).
9. Bernard A, Gain P, Mauclair C et al. Device and method for cutting a cornea or crystalline lens. (2017). https://eureka-patsnap-com.libproxy1.nus.edu.sg/patent-US20170304118A1.
10. Taylor R, Hnatovsky C, Simova E. Applications of femtosecond laser induced self-organized planar nanocracks inside fused silica glass. *Laser Photonics Rev* **2**, 26–46 (2008).
11. Bonse J, Krüger J, Höhm S et al. Femtosecond laser-induced periodic surface structures. *J Laser Appl* **24**, 042006 (2012).
12. Nolte S, Momma C, Jacobs H et al. Ablation of metals by ultrashort laser pulses. *J Opt Soc Am B* **14**, 2716–2722 (1997).
13. Neuenschwander B, Jaeggi B, Schmid M et al. Surface structuring with ultra-short laser pulses: basics, limitations and needs for high throughput. *Phys Procedia* **56**, 1047–1058 (2014).
14. Bellouard Y, Said A, Dugan M et al. Fabrication of high-aspect ratio, micro-fluidic channels and tunnels using femtosecond laser pulses and chemical etching. *Opt Express* **12**, 2120–2129 (2004).
15. Mishchik K, Cheng G, Huo G et al. Nanosize structural modifications with polarization functions in ultrafast laser irradiated bulk fused silica. *Opt Express* **18**, 24809–24824 (2010).
16. Wu D, Wu SZ, Xu J et al. Hybrid femtosecond laser microfabrication to achieve true 3D glass/polymer composite biochips with multiscale features and high performance: the concept of ship-in-a-bottle biochip. *Laser Photonics Rev* **8**, 458–467 (2014).
17. Colombier JP, Combis P, Bonneau F et al. Hydrodynamic simulations of metal ablation by femtosecond laser irradiation. *Phys Rev B* **71**, 165406 (2005).
18. Ahmmed KMT, Ling EJY, Servio P et al. Introducing a new optimization tool for femtosecond laser-induced surface texturing on titanium, stainless steel, aluminum and copper. *Opt Lasers Eng* **66**, 258–268 (2015).
19. Sedao X, Lenci M, Rudenko A et al. Influence of pulse repetition rate on morphology and material removal rate of ultrafast laser ablated metallic surfaces. *Opt Lasers Eng* **116**, 68–74 (2019).
20. Shin H, Kim D. Cutting thin glass by femtosecond laser ablation. *Opt Laser Technol* **102**, 1–11 (2018).
21. Pietroy D, Baubeau E, Faure N et al. Intensity profile distortion at the processing image plane of a focused femtosecond laser below the critical power: analysis and counteraction. *Opt Lasers Eng* **66**, 138–143 (2015).
22. Mauclair C, Mermillod-Blondin A, Landon S et al. Single-pulse ultrafast laser imprinting of axial dot arrays in bulk glasses. *Opt Lett* **36**, 325–327 (2011).
23. Le Harzic R, Huot N, Audouard E et al. Comparison of heat-affected zones due to nanosecond and femtosecond laser pulses using transmission electronic microscopy. *Appl Phys Lett* **80**, 3886–3888 (2002).
24. Bauer F, Michalowski A, Kiedrowski T et al. Heat accumulation in ultra-short pulsed scanning laser ablation of metals. *Opt Express* **23**, 1035–1043 (2015).
25. Eaton SM, Zhang HB, Herman PR et al. Heat accumulation effects in femtosecond laser-written waveguides with variable repetition rate. *Opt Express* **13**, 4708–4716 (2005).
26. Emelyanenko AM, Shagieva FM, Domantovsky AG et al. Nanosecond laser micro- and nanotexturing for the design of a superhydrophobic coating robust against long-term contact with water, cavitation, and abrasion. *Appl Surf Sci* **332**, 513–517 (2015).
27. Ancona A, Röser F, Rademaker K et al. High speed laser drilling of metals using a high repetition rate, high average power ultrafast fiber CPA system. *Opt Express* **16**, 8958–8968 (2008).
28. Neuenschwander B, Jaeggi B, Zimmermannn M et al. Laser surface structuring with 100 W of average power and sub-ps pulses. *J Laser Appl* **28**, 022506 (2016).
29. Loeschner U, Schille J, Streek A et al. High-rate laser microprocessing using a polygon scanner system. *J Laser Appl* **27**, S29303 (2015).
30. Römer GRBE, Bechtold P. Electro-optic and acousto-optic laser beam scanners. *Phys Procedia* **56**, 29–39 (2014).
31. Kerse C, Kalaycıoğlu H, Elahi P et al. Ablation-cooled material removal with ultrafast bursts of pulses. *Nature* **537**, 84–88 (2016).
32. Audouard E, Mottay E. High efficiency GHz laser processing with long bursts. *Int J Extrem Manuf* **5**, 015003 (2023).
33. Nyenhuis F, Michalowski A, L'huillier J. Surface treatment with GHz bursts. *Proc SPIE* **11268**, 112680B (2020).
34. Dahmen M, Güdükkurt O, Kaierle S. The ecological footprint of laser beam welding. *Phys Procedia* **5**, 19–28 (2010).
35. Sanner N, Huot N, Audouard E et al. Programmable focal spot shaping of amplified femtosecond laser pulses. *Opt Lett* **30**, 1479–1481 (2005).
36. Hasegawa S, Hayasaki Y, Nishida N. Holographic femtosecond laser processing with multiplexed phase Fresnel lenses. *Opt Lett* **31**, 1705–1707 (2006).
37. Kuang Z, Perrie W, Leach J et al. High throughput diffractive multi-beam femtosecond laser processing using a spatial light modulator. *Appl Surf Sci* **255**, 2284–2289 (2008).
38. Massachusetts Institute of Technology. Archimedes Death Ray: Idea Feasibility Testing. [2025-01-15] https://web.mit.edu/2.009_gallery/www/2005_other/archimedes/10_ArchimedesResult.html
39. Strobel V. Pold87/academic-keyword-occurrence: first release (Zenodo, 2018). doi: 10.5281/zenodo.1218409.
40. Siegman AE. *Lasers* 2nd ed (University Science Books, 1990).
41. Diels JC, Rudolph W. *Ultrashort Laser Pulse Phenomena: Fundamentals, Techniques, and Applications on a Femtosecond Time Scale* 2nd ed (Academic Press Inc., Burlington, 2006).
42. Goodman JW. *Introduction to Fourier Optics* 3rd ed (Roberts & Company Publishers, Englewood, 2005).
43. Ams M, Marshall GD, Spence DJ et al. Slit beam shaping method for femtosecond laser direct-write fabrication of symmetric waveguides in bulk glasses. *Opt Express* **13**, 5676–5681 (2005).
44. Kuang Z, Li JN, Edwardson S et al. Ultrafast laser beam shap-

ing for material processing at imaging plane by geometric masks using a spatial light modulator. *Opt Lasers Eng* **70**, 1–5 (2015).
45. Malitson IH. Interspecimen comparison of the refractive index of fused silica. *J Opt Soc Am* **55**, 1205–1209 (1965).
46. Torres-Peiró S, González-Ausejo J, Mendoza-Yero O et al. Parallel laser micromachining based on diffractive optical elements with dispersion compensated femtosecond pulses. *Opt Express* **21**, 31830–31836 (2013).
47. Amako J, Nagasaka K, Kazuhiro N. Chromatic-distortion compensation in splitting and focusing of femtosecond pulses by use of a pair of diffractive optical elements. *Opt Lett* **27**, 969–971 (2002).
48. Hasegawa S, Ito H, Toyoda H et al. Massively parallel femtosecond laser processing. *Opt Express* **24**, 18513–18524 (2016).
49. Yang YQ, Forbes A, Cao LC. A review of liquid crystal spatial light modulators: devices and applications. *Opto-Electron Sci* **2**, 230026 (2023).
50. Salter PS, Booth MJ. Adaptive optics in laser processing. *Light Sci Appl* **8**, 110 (2019).
51. Malinauskas M, Žukauskas A, Hasegawa S et al. Ultrafast laser processing of materials: from science to industry. *Light Sci Appl* **5**, e16133 (2016).
52. Aubourg P, Huignard JP, Hareng M et al. Liquid crystal light valve using bulk monocrystalline $Bi_{12}SiO_{20}$ as the photoconductive material. *Appl Opt* **21**, 3706–3712 (1982).
53. Zhu G, Whitehead D, Perrie W et al. Investigation of the thermal and optical performance of a spatial light modulator with high average power picosecond laser exposure for materials processing applications. *J Phys D: Appl Phys* **51**, 095603 (2018).
54. Hasegawa S, Nozaki K, Tanabe A et al. Holographic femtosecond laser processing using 6.3 kHz pulse-to-pulse spatial light modulation with binary phase masks. *Opt Laser Technol* **176**, 111014 (2024).
55. Smarra M, Gurevich EL, Ostendorf A. Theoretical simulation and experimental verification of dynamic caustic manipulation using a deformable mirror for laser material processing. *Opt Laser Technol* **149**, 107814 (2022).
56. El-Agmy R, Bulte H, Greenaway AH et al. Adaptive beam profile control using a simulated annealing algorithm. *Opt Express* **13**, 6085–6091 (2005).
57. Scholes S, Mohapi L, Leach J et al. Experimentally simulating the beam shaping capabilities of piston-type deformable mirrors using a liquid crystal spatial light modulator. *Appl Phys B* **129**, 45 (2023).
58. Ren YX, Lu RD, Gong L. Tailoring light with a digital micromirror device. *Ann Phys* **527**, 447–470 (2015).
59. Trypogeorgos D, Harte T, Bonnin A et al. Precise shaping of laser light by an acousto-optic deflector. *Opt Express* **21**, 24837–24846 (2013).
60. Häfner T, Strauß J, Roider C et al. Tailored laser beam shaping for efficient and accurate microstructuring. *Appl Phys A* **124**, 111 (2018).
61. Fontaine NK, Ryf R, Chen HS et al. Laguerre-gaussian mode sorter. *Nat Commun* **10**, 1865 (2019).
62. Labroille G, Denolle B, Jian P et al. Efficient and mode selective spatial mode multiplexer based on multi-plane light conversion. *Opt Express* **22**, 15599–15607 (2014).
63. Meunier M, Kumar A, Lucas A et al. Stainless steel laser beam welding with a dynamic tailored beam shaping laser-head based on multi-plane light conversion. *Proc SPIE* **PC12414**, PC1241407 (2023).
64. Jacquard C, Placzek K, Holder D et al. Microprocessing with a multi-plane light conversion beam shaper and a femtosecond laser at 515nm. *Proc SPIE* **12409**, 1240910 (2023).
65. Palima D, Glückstad J. Gaussian to uniform intensity shaper based on generalized phase contrast. *Opt Express* **16**, 1507–1516 (2008).
66. Tauro S, Bañas A, Palima D et al. Experimental demonstration of Generalized Phase Contrast based Gaussian beam-shaper. *Opt Express* **19**, 7106–7111 (2011).
67. Zernike VF. Beugungstheorie des schneidenver-fahrens und seiner verbesserten form, der phasenkontrastmethode. *Physica* **1**, 689–704 (1934).
68. Bañas A, Kopylov O, Villangca M et al. GPC light shaper: static and dynamic experimental demonstrations. *Opt Express* **22**, 23759–23769 (2014).
69. Eriksen RL, Mogensen PC, Glückstad J. Multiple-beam optical tweezers generated by the generalized phase-contrast method. *Opt Lett* **27**, 267–269 (2002).
70. Lasagni A, Roch T, Bieda M et al. High speed surface functionalization using direct laser interference patterning, towards 1 m^2/min fabrication speed with sub-micrometric resolution. *Proc SPIE* **8968**, 89680A (2014).
71. Zhou Q, Yang WZ, He FT et al. Femtosecond multi-beam interference lithography based on dynamic wavefront engineering. *Opt Express* **21**, 9851–9861 (2013).
72. Li BH, Jiang L, Li XW et al. Flexible gray-scale surface patterning through spatiotemporal-interference-based femtosecond laser shaping. *Adv Opt Mater* **6**, 1801021 (2018).
73. Wu H, Jiao YL, Zhang CC et al. Large area metal micro-/nanogroove arrays with both structural color and anisotropic wetting fabricated by one-step focused laser interference lithography. *Nanoscale* **11**, 4803–4810 (2019).
74. Madelung A, Alamri S, Steege T et al. Scanner-based direct laser interference patterning on stainless steel. *Adv Eng Mater* **23**, 2001414 (2021).
75. Rank A, Lang V, Lasagni AF. High-speed roll-to-roll hot embossing of micrometer and sub micrometer structures using seamless direct laser interference patterning treated sleeves. *Adv Eng Mater* **19**, 1700201 (2017).
76. McLeod E, Hopkins AB, Arnold CB. Multiscale Bessel beams generated by a tunable acoustic gradient index of refraction lens. *Opt Lett* **31**, 3155–3157 (2006).
77. Duocastella M, Arnold CB. Enhanced depth of field laser processing using an ultra-high-speed axial scanner. *Appl Phys Lett* **102**, 061113 (2013).
78. Du XH, Florian C, Arnold CB. Single-lens dynamic *z*-scanning for simultaneous in situ position detection and laser processing focus control. *Light Sci Appl* **12**, 274 (2023).
79. Toporovsky V, Samarkin V, Sheldakova J et al. Water-cooled stacked-actuator flexible mirror for high-power laser beam correction. *Opt Laser Technol* **144**, 107427 (2021).
80. Chorel M, Lanternier T, Lavastre É et al. Robust optimization of the laser induced damage threshold of dielectric mirrors for high power lasers. *Opt Express* **26**, 11764–11774 (2018).
81. Ramousse L, Chériaux G, Claudet C et al. Femtosecond laser-induced damage threshold of nematic liquid crystals at 1030

nm. *Appl Opt* **60**, 8050–8056 (2021).
82. Xing ZB, Fan W, Huang DJ et al. High laser damage threshold liquid crystal optical switch based on a gallium nitride transparent electrode. *Opt Lett* **45**, 3537–3540 (2020).
83. LCOS-Slm Applications and Features Cat. No. LLAP3012E05 Hamamatsu Photonics. 2025. https://lcos-slm.hamamatsu.com/eu/en/related-contents.html.
84. Tang Y, Li QL, Fang Z et al. Extending the operational limit of a cooled spatial light modulator exposed to 200W average power for holographic picosecond laser materials processing. *Opt Laser Technol* **181**, 111589 (2025).
85. Maingot B, Neradovskaia E, Claudet C et al. Measurement of nonlinear refractive indices of bulk and liquid crystals by nonlinear chirped interferometry. *Opt Lett* **48**, 3243–3246 (2023).
86. Duclère JR, Hayakawa T, Roginskii EM et al. Third order nonlinear optical properties of a paratellurite single crystal. *J Appl Phys* **123**, 183105 (2018).
87. Gerchberg RW, Saxton WO. A practical algorithm for the determination of phase from image and diffraction plane pictures. *Optik* **35**, 237–246 (1972).
88. Sinclair G, Leach J, Jordan P et al. Interactive application in holographic optical tweezers of a multi-plane Gerchberg-saxton algorithm for three-dimensional light shaping. *Opt Express* **12**, 1665–1670 (2004).
89. Di Leonardo R, Ianni F, Ruocco G. Computer generation of optimal holograms for optical trap arrays. *Opt Express* **15**, 1913–1922 (2007).
90. Silvennoinen M, Kaakkunen J, Paivasaari K et al. Parallel femtosecond laser ablation with individually controlled intensity. *Opt Express* **22**, 2603–2608 (2014).
91. Gaunt AL, Hadzibabic Z. Robust digital holography for ultracold atom trapping. *Sci Rep* **2**, 721 (2012).
92. van Bijnen RMW, Ravensbergen C, Bakker DJ et al. Patterned Rydberg excitation and ionization with a spatial light modulator. *New J Phys* **17**, 023045 (2015).
93. Liesener J, Reicherter M, Haist T et al. Multi-functional optical tweezers using computer-generated holograms. *Opt Commun* **185**, 77–82 (2000).
94. Leach J, Wulff K, Sinclair G et al. Interactive approach to optical tweezers control. *Appl Opt* **45**, 897–903 (2006).
95. Jesacher A, Booth MJ. Parallel direct laser writing in three dimensions with spatially dependent aberration correction. *Opt Express* **18**, 21090–21099 (2010).
96. Bengtsson J. Kinoform design with an optimal-rotation-angle method. *Appl Opt* **33**, 6879–6884 (1994).
97. Dammann H, Klotz E. Coherent optical generation and inspection of two-dimensional periodic structures. *Opt Acta: Int J Opt* **24**, 505–515 (1977).
98. Yu JJ, Zhou CH, Jia W et al. Three-dimensional Dammann array. *Appl Opt* **51**, 1619–1630 (2012).
99. Zhu LW, Yu JJ, Zhang DW et al. Multifocal spot array generated by fractional talbot effect phase-only modulation. *Opt Express* **22**, 9798–9808 (2014).
100. Wright AJ, Burns D, Patterson BA et al. Exploration of the optimisation algorithms used in the implementation of adaptive optics in confocal and multiphoton microscopy. *Micros Res Tech* **67**, 36–44 (2005).
101. Mauclair C, Mermillod-Blondin A, Huot N et al. Ultrafast laser writing of homogeneous longitudinal waveguides in glasses using dynamic wavefront correction. *Opt Express* **16**, 5481–5492 (2008).
102. Hauschwitz P, Brajer J, Rostohar D et al. Anti-reflection nanostructures on tempered glass by dynamic beam shaping. *Micromachines* **12**, 289 (2021).
103. Saint-Pierre D, Granier J, Egaud G et al. Fast uniform micro structuring of DLC surfaces using multiple ultrashort laser spots through spatial beam shaping. *Phys Procedia* **83**, 1178–1183 (2016).
104. Parry JP, Beck RJ, Shephard JD et al. Application of a liquid crystal spatial light modulator to laser marking. *Appl Opt* **50**, 1779–1785 (2011).
105. Wang ZP, Jiang L, Li XW et al. High efficiency and scalable fabrication of fresnel zone plates using holographic femtosecond pulses. *Nanophotonics* **11**, 3081–3091 (2022).
106. Kato J, Takeyasu N, Adachi Y et al. Multiple-spot parallel processing for laser micronanofabrication. *Appl Phys Lett* **86**, 044102 (2005).
107. Sipe JE, Young JF, Preston JS et al. Laser-induced periodic surface structure. I. theory. *Phys Rev B* **27**, 1141–1154 (1983).
108. Han RZ, Zhang YC, Jiang QL et al. Ultrafast dynamics of femtosecond laser-induced high spatial frequency periodic structures on silicon surfaces. *Opto-Electron Sci* **3**, 230013 (2024).
109. Dusser B, Sagan Z, Soder H et al. Controlled nanostructrures formation by ultra fast laser pulses for color marking. *Opt Express* **18**, 2913–2924 (2010).
110. Hendriks A, Naidoo D, Roux FS et al. The generation of flattop beams by complex amplitude modulation with a phase-only spatial light modulator. *Proc SPIE* **8490**, 849006 (2012).
111. Mauclair C, Saint-Pierre D, Desrus H. Advances in spatial beam shaping for ultrafast laser surface functionalization. In *Proceedings of the Lasers in Manufacturing Conference 2017* (2017).
112. Mourier L, Mazuyer D, Lubrecht AA et al. Action of a femtosecond laser generated micro-cavity passing through a circular EHL contact. *Wear* **264**, 450–456 (2008).
113. Dong ZL, Sun XY, Kong DJ et al. Spatial light modulated femtosecond laser ablated durable superhydrophobic copper mesh for oil-water separation and self-cleaning. *Surf Coat Technol* **402**, 126254 (2020).
114. Mauclair C, Pietroy D, Di Maïo Y et al. Ultrafast laser microcutting of stainless steel and PZT using a modulated line of multiple foci formed by spatial beam shaping. *Opt Lasers Eng* **67**, 212–217 (2015).
115. Laskin A, Laskin V. Refractive beam shapers for material processing with high power single mode and multimode lasers. *Proc SPIE* **8600**, 860010 (2013).
116. Schlutow H, Fuchs U, Müller FA et al. Squared focal intensity distributions for applications in laser material processing. *Materials* **14**, 4981 (2021).
117. Sanner N. Mise en forme programmable de faisceau laser femtoseconde pour le micro-usinage et la photoinscription de guides d'ondes (Université Jean Monnet, Saint-Etienne, 2005).
118. Guillon M, Forget BC, Foust AJ et al. Vortex-free phase profiles for uniform patterning with computer-generated holography. *Opt Express* **25**, 12640–12652 (2017).
119. Yuan YJ, Jiang L, Li X et al. Laser photonic-reduction stamping for graphene-based micro-supercapacitors ultrafast fabrication. *Nat Commun* **11**, 6185 (2020).
120. Hasegawa S, Shiono K, Hayasaki Y. Femtosecond laser processing with a holographic line-shaped beam. *Opt Express* **23**,

23185–23194 (2015).
121. Hasegawa S, Ito H, Toyoda H et al. Diffraction-limited ring beam generated by radial grating. *OSA Continuum* **1**, 283–294 (2018).
122. Wang J, Hayasaki Y, Zhang FY et al. Three-dimensional holographic femtosecond laser parallel processing method with the fractional Fourier transform for glass substrates. *Ceram Int* **48**, 16364–16373 (2022).
123. de Saint Jean A, Dufournel D, Stodulka P et al. Comparison of ultrasound phacoemulsification and FemtoMatrix® PhotoEmulsification® cataract surgery. *Front Med* **10**, 1157486 (2023).
124. Mauclair C, Cheng G, Huot N et al. Dynamic ultrafast laser spatial tailoring for parallel micromachining of photonic devices in transparent materials. *Opt Express* **17**, 3531–3542 (2009).
125. Cumming BP, Turner MD, Schröder-Turk GE et al. Adaptive optics enhanced direct laser writing of high refractive index gyroid photonic crystals in chalcogenide glass. *Opt Express* **22**, 689–698 (2014).
126. Cumming BP, Jesacher A, Booth MJ et al. Adaptive aberration compensation for three-dimensional micro-fabrication of photonic crystals in lithium niobate. *Opt Express* **19**, 9419–9425 (2011).
127. Sun BS, Salter PS, Booth MJ. High conductivity micro-wires in diamond following arbitrary paths. *Appl Phys Lett* **105**, 231105 (2014).
128. Xu K, Huang PL, Huang LY et al. High-precision multi-focus laser sculpting of microstructured glass. *Opto-Electron Adv* **7**, 240082 (2024).
129. Vellekoop IM, Mosk AP. Focusing coherent light through opaque strongly scattering media. *Opt Lett* **32**, 2309–2311 (2007).
130. Galaktionov I, Nikitin A, Sheldakova J et al. Focusing of a laser beam passed through a moderately scattering medium using phase-only spatial light modulator. *Photonics* **9**, 296 (2022).
131. Jayasinghe AK, Rohner J, Hutson MS. Holographic UV laser microsurgery. *Biomed Opt Express* **2**, 2590–2599 (2011).
132. Vargas-Martín F, Prieto PM, Artal P. Correction of the aberrations in the human eye with a liquid-crystal spatial light modulator: limits to performance. *J Opt Soc Am A* **15**, 2552–2562 (1998).
133. Sinjab F, Liao ZY, Notingher I. Applications of spatial light modulators in Raman spectroscopy. *Appl Spectrosc* **73**, 727–746 (2019).
134. Carnegie DJ, Čižmár T, Baumgartl J et al. Automated laser guidance of neuronal growth cones using a spatial light modulator. *J Biophotonics* **2**, 682–692 (2009).
135. Ocier CR, Richards CA, Bacon-Brown DA et al. Direct laser writing of volumetric gradient index lenses and waveguides. *Light Sci Appl* **9**, 196 (2020).
136. Ochiai Y, Kumagai K, Hoshi T et al. Fairy lights in femtoseconds: aerial and volumetric graphics rendered by focused femtosecond laser combined with computational holographic fields. *ACM Trans Graph* **35**, 17 (2016).
137. Bhuyan MK, Courvoisier F, Lacourt PA et al. High aspect ratio nanochannel machining using single shot femtosecond Bessel beams. *Appl Phys Lett* **97**, 081102 (2010).
138. Belloni VV, Hassan M, Furfaro L et al. Single shot generation of high-aspect-ratio nano-rods from sapphire by ultrafast first order Bessel beam. *Laser Photonics Rev* **18**, 2300687 (2024).
139. Mathis A, Courvoisier F, Froehly L et al. Micromachining along a curve: femtosecond laser micromachining of curved profiles in diamond and silicon using accelerating beams. *Appl Phys Lett* **101**, 071110 (2012).
140. Xie C, Jukna V, Milián C et al. Tubular filamentation for laser material processing. *Sci Rep* **5**, 8914 (2015).
141. Flamm D, Grossmann DG, Sailer M et al. Structured light for ultrafast laser micro- and nanoprocessing. *Opt Eng* **60**, 025105 (2021).
142. Dat Nguyen H, Moreno E, Rudenko A et al. Super-efficient drilling of metals with ultrafast non diffractive laser beams. *Sci Rep* **12**, 2074 (2022).
143. Yu XM, Trallero-Herrero CT, Lei ST. Materials processing with superposed Bessel beams. *Appl Surf Sci* **360**, 833–839 (2016).
144. Courvoisier F, Lacourt PA, Jacquot M et al. Surface nanoprocessing with nondiffracting femtosecond Bessel beams. *Opt Lett* **34**, 3163–3165 (2009).
145. Fahrbach FO, Simon P, Rohrbach A. Microscopy with self-reconstructing beams. *Nat Photonics* **4**, 780–785 (2010).
146. Simon DS. Bessel beams, self-healing, and diffraction-free propagation. In Simon DS. *A Guided Tour of Light Beams: From Lasers to Optical Knots* (Morgan & Claypool Publishers, San Rafael, 2016); http://doi.org/10.1088/978-1-6817-4437-7ch5.
147. Mishchik K, Beuton R, Caulier OD et al. Improved laser glass cutting by spatio-temporal control of energy deposition using bursts of femtosecond pulses. *Opt Express* **25**, 33271–33282 (2017).
148. Osbild M, Gerhorst EA, Sivankutty S et al. Submicrometer surface structuring with a Bessel beam generated by a reflective axicon. *J Laser Appl* **33**, 042013 (2021).
149. D'Amico C, Martin G, Troles J et al. Multiscale laser written photonic structures in bulk chalcogenide glasses for infrared light transport and extraction. *Photonics* **8**, 211 (2021).
150. Tamaki T, Watanabe W, Nishii J et al. Welding of transparent materials using femtosecond laser pulses. *Jpn J Appl Phys* **44**, L687 (2005).
151. Tan DZ, Zhang B, Qiu JR. Ultrafast laser direct writing in glass: thermal accumulation engineering and applications. *Laser Photonics Rev* **15**, 2000455 (2021).
152. Zhang GD, Stoian R, Zhao W et al. Femtosecond laser Bessel beam welding of transparent to non-transparent materials with large focal-position tolerant zone. *Opt Express* **26**, 917–926 (2018).
153. Zhang GD, Pan Y, Wu PF et al. Glass micro welding in thermal accumulation regime with using spatially shaped ultrafast laser. *Opt Laser Technol* **168**, 109845 (2024).
154. Baltrukonis J, Ulčinas O, Orlov S et al. High-order vector Bessel-gauss beams for laser micromachining of transparent materials. *Phys Rev Appl* **16**, 034001 (2021).
155. Alimohammadian E, Ertorer E, Uzeda EM et al. Inhibition and enhancement of linear and nonlinear optical effects by conical phase front shaping for femtosecond laser material processing. *Sci Rep* **10**, 21528 (2020).
156. Ganguly N, Dwivedi R, D'Amico C et al. Asymmetric shaping for ultrafast elliptical bessel-like beams. *Photonics* **10**, 651 (2023).
157. Ouyang J, Perrie W, Allegre OJ et al. Tailored optical vector fields for ultrashort-pulse laser induced complex surface plas-

mon structuring. *Opt Express* **23**, 12562–12572 (2015).
158. Hasegawa S, Hayasaki Y. Polarization distribution control of parallel femtosecond pulses with spatial light modulators. *Opt Express* **21**, 12987–12995 (2013).
159. Hong JT, Li J, Chu DP. Efficient dynamic control method of light polarization using single phase-only liquid crystal on silicon spatial light modulators for optical data storage. *Appl Opt* **61**, B34–B42 (2022).
160. Li ZQ, Allegre O, Li L. Realising high aspect ratio 10 nm feature size in laser materials processing in air at 800 nm wavelength in the far-field by creating a high purity longitudinal light field at focus. *Light Sci Appl* **11**, 339 (2022).
161. Zeng TT, Chang CL, Chen ZZ et al. Three-dimensional vectorial multifocal arrays created by pseudo-period encoding. *J Opt* **20**, 065605 (2018).
162. Li P, Fan XH, Wu DJ et al. Shaping vector fields in three dimensions by random Fourier phase-only encoding. *Opt Express* **27**, 30009–30019 (2019).
163. Freidank S, Vogel A, Linz N. Optical vortex beam for gentle and ultraprecise intrastromal corneal dissection in refractive surgery. *Trans Vis Sci Technol* **9**, 22 (2020).
164. Yao AM, Padgett MJ. Orbital angular momentum: origins, behavior and applications. *Adv Opt Photonics* **3**, 161–204 (2011).
165. Allegre OJ, Jin Y, Perrie W et al. Complete wavefront and polarization control for ultrashort-pulse laser microprocessing. *Opt Express* **21**, 21198–21207 (2013).
166. Jin Y, Allegre OJ, Perrie W et al. Dynamic modulation of spatially structured polarization fields for real-time control of ultrafast laser-material interactions. *Opt Express* **21**, 25333–25343 (2013).
167. Ghosal A, Allegre OJ, Liu Z et al. Surface engineering with structured femtosecond laser vector fields. *Results Opt* **5**, 100179 (2021).
168. Skoulas E, Manousaki A, Fotakis C et al. Biomimetic surface structuring using cylindrical vector femtosecond laser beams. *Sci Rep* **7**, 45114 (2017).
169. Gu M, Li XP, Cao YY. Optical storage arrays: a perspective for future big data storage. *Light Sci Appl* **3**, e177 (2014).
170. Lu JF, Hassan M, Courvoisier F et al. 3D structured Bessel beam polarization and its application to imprint chiral optical properties in silica. *APL Photonics* **8**, 060801 (2023).
171. Freidank S, Vogel A, Linz N. Mechanisms of corneal intrastromal laser dissection for refractive surgery: ultra-high-speed photographic investigation at up to 50 million frames per second. *Biomed Opt Express* **13**, 3056–3079 (2022).
172. Yang L, Li JW, Hu YL et al. Projection two-photon polymerization using a spatial light modulator. *Opt Commun* **331**, 82–86 (2014).
173. Yang L, El-Tamer A, Hinze U et al. Parallel direct laser writing of micro-optical and photonic structures using spatial light modulator. *Opt Lasers Eng* **70**, 26–32 (2015).
174. Somers P, Liang ZH, Johnson JE et al. Rapid, continuous projection multi-photon 3D printing enabled by spatiotemporal focusing of femtosecond pulses. *Light Sci Appl* **10**, 199 (2021).
175. Heath DJ, Feinaeugle M, Grant-Jacob JA et al. Dynamic spatial pulse shaping via a digital micromirror device for patterned laser-induced forward transfer of solid polymer films. *Opt Mater Express* **5**, 1129–1136 (2015).
176. Fischer J, Wegener M. Three-dimensional direct laser writing inspired by stimulated-emission-depletion microscopy [Invited]. *Opt Mater Express* **1**, 614–624 (2011).
177. Ni JC, Wang CW, Zhang CC et al. Three-dimensional chiral microstructures fabricated by structured optical vortices in isotropic material. *Light Sci Appl* **6**, e17011 (2017).
178. Dat Nguyen H, Sedao X, Mauclair C et al. Non-diffractive Bessel beams for ultrafast laser scanning platform and proof-of-concept side-wall polishing of additively manufactured parts. *Micromachines* **11**, 974 (2020).
179. Ergin T, Stenger N, Brenner P et al. Three-dimensional invisibility cloak at optical wavelengths. *Science* **328**, 337–339 (2010).
180. in't Veld BH, Overmeyer L, Schmidt M et al. Micro additive manufacturing using ultra short laser pulses. *CIRP Ann* **64**, 701–724 (2015).
181. Saunders J, Elbestawi M, Fang QY. Ultrafast laser additive manufacturing: a review. *J Manuf Mater Process* **7**, 89 (2023).
182. Schmidt M, Cvecek K, Duflou J et al. Dynamic beam shaping —Improving laser materials processing via feature synchronous energy coupling. *CIRP Ann* **73**, 533–559 (2024).
183. Geng Q, Wang DE, Chen PF et al. Ultrafast multi-focus 3-D nano-fabrication based on two-photon polymerization. *Nat Commun* **10**, 2179 (2019).
184. Auyeung RCY, Kim H, Mathews S et al. Laser forward transfer using structured light. *Opt Express* **23**, 422–430 (2015).
185. Thiel M, Fischer J, von Freymann G et al. Direct laser writing of three-dimensional submicron structures using a continuous-wave laser at 532 nm. *Appl Phys Lett* **97**, 221102 (2010).
186. Batchelor R, Messer T, Hippler M et al. Two in one: light as a tool for 3D printing and erasing at the microscale. *Adv Mater* **31**, 1904085 (2019).
187. Xiong W, Zhou YS, He XN et al. Simultaneous additive and subtractive three-dimensional nanofabrication using integrated two-photon polymerization and multiphoton ablation. *Light Sci Appl* **1**, e6 (2012).
188. Malinauskas M, Rekštytė S, Lukoševičius L et al. 3D microporous scaffolds manufactured via combination of fused filament fabrication and direct laser writing ablation. *Micromachines* **5**, 839–858 (2014).
189. Hell SW, Wichmann J. Breaking the diffraction resolution limit by stimulated emission: stimulated-emission-depletion fluorescence microscopy. *Opt Lett* **19**, 780–782 (1994).
190. Rittweger E, Han KY, Irvine SE et al. STED microscopy reveals crystal colour centres with nanometric resolution. *Nat Photonics* **3**, 144–147 (2009).
191. Pereira A, Sousa M, Almeida AC et al. Coherent-hybrid STED: high contrast sub-diffraction imaging using a bi-vortex depletion beam. *Opt Express* **27**, 8092–8111 (2019).
192. Hahn V, Rietz P, Hermann F et al. Light-sheet 3D microprinting via two-colour two-step absorption. *Nat Photonics* **16**, 784–791 (2022).
193. Nakamura R, Kawaguchi H, Iwata M et al. Optical vortex-induced forward mass transfer: manifestation of helical trajectory of optical vortex. *Opt Express* **27**, 38019–38027 (2019).
194. Kaneko A, Iwata M, Wei R et al. Using optical vortex laser induced forward transfer to fabricate a twisted ferrite microcrystal array. *APL Mater* **12**, 061116 (2024).
195. Nie B, Huang H, Bai S et al. Femtosecond laser melting and resolidifying of high-temperature powder materials. *Appl Phys A* **118**, 37–41 (2015).
196. Kaden L, Matthäus G, Ullsperger T et al. Selective laser melt-

ing of copper using ultrashort laser pulses. *Appl Phys A* **123**, 596 (2017).
197. Kaligar AB, Kumar HA, Ali A et al. Femtosecond laser-based additive manufacturing: current status and perspectives. *Quantum Beam Sci* **6**, 5 (2022).
198. Mingareev I, Bonhoff T, El-Sherif AF et al. Femtosecond laser post-processing of metal parts produced by laser additive manufacturing. *J Laser Appl* **25**, 052009 (2013).
199. Worts N, Jones J, Squier J. Surface structure modification of additively manufactured titanium components via femtosecond laser micromachining. *Opt Commun* **430**, 352–357 (2019).
200. Chaen K, Takahashi H, Hasegawa S et al. Display method with compensation of the spatial frequency response of a liquid crystal spatial light modulator for holographic femtosecond laser processing. *Opt Commun* **280**, 165–172 (2007).
201. Ackermann L, Roider C, Gehring M et al. High-speed speckle averaging for phase-only beam shaping in laser materials processing. *Opt Lasers Eng* **165**, 107537 (2023).
202. Schroff P, La Rooij A, Haller E et al. Accurate holographic light potentials using pixel crosstalk modelling. *Sci Rep* **13**, 3252 (2023).
203. Hayasaki Y, Onodeara R, Kumagai K et al. Automatic generation of a holographically shaped beam in an actual optical system for use in material laser processing. *Opt Express* **31**, 1982–1991 (2023).
204. Houzet J, Faure N, Larochette M, et al. Ultrafast laser spatial beam shaping based on zernike polynomials for surface processing. *Opt Express* **24**, 6542–6552 (2016).
205. Lazarev G, Chen PJ, Strauss J et al. Beyond the display: phase-only liquid crystal on silicon devices and their applications in photonics [Invited]. *Opt Express* **27**, 16206–16249 (2019).
206. Kuang Z, Liu D, Perrie W et al. Fast parallel diffractive multi-beam femtosecond laser surface micro-structuring. *Appl Surf Sci* **255**, 6582–6588 (2009).
207. Kuang Z, Perrie W, Liu D et al. Diffractive multi-beam surface micro-processing using 10 ps laser pulses. *Appl Surf Sci* **255**, 9040–9044 (2009).
208. Wang J, Sun SF, Zhang HH et al. Holographic femtosecond laser parallel processing method based on the fractional Fourier transform. *Opt Lasers Eng* **146**, 106704 (2021).
209. Ronzitti E, Guillon M, de Sars V et al. LCoS nematic SLM characterization and modeling for diffraction efficiency optimization, zero and ghost orders suppression. *Opt Express* **20**, 17843–17855 (2012).
210. Prossotowicz M, Flamm D, Heimes A et al. Dynamic focus shaping with mixed-aperture coherent beam combining. *Opt Lett* **46**, 1660–1663 (2021).
211. Arrizón V, Ruiz U, Carrada R et al. Pixelated phase computer holograms for the accurate encoding of scalar complex fields. *J Opt Soc Am A* **24**, 3500–3507 (2007).
212. Wang ZP, Li XW, Jiang L et al. High-quality micropattern printing by interlacing-pattern holographic femtosecond pulses. *Nanophotonics* **9**, 2895–2904 (2020).
213. Mauclair C, Landon S, Pietroy D et al. Ultrafast laser machining of micro grooves on stainless steel with spatially optimized intensity distribution. *J Laser Micro Nanoeng* **8**, 11–14 (2013).
214. Chang CL, Xia J, Yang L et al. Speckle-suppressed phase-only holographic three-dimensional display based on double-constraint Gerchberg-Saxton algorithm. *Appl Opt* **54**, 6994–7001 (2015).
215. Ackermann L, Roider C, Cvecek K et al. Methods for uniform beam shaping and their effect on material ablation. *Appl Phys A* **128**, 877 (2022).
216. Kim D, Keesling A, Omran A et al. Large-scale uniform optical focus array generation with a phase spatial light modulator. *Opt Lett* **44**, 3178–3181 (2019).
217. Bañas A, Glückstad J. Light shaping with holography, GPC and holo-GPC. *Opt Data Process Storage* **3**, 20–40 (2017).
218. Nakata Y, Osawa K, Miyanaga N. Utilization of the high spatial-frequency component in adaptive beam shaping by using a virtual diagonal phase grating. *Sci Rep* **9**, 4640 (2019).
219. Madsen AEG, Eriksen RL, Glückstad J. Comparison of state-of-the-art Computer Generated Holography algorithms and a machine learning approach. *Opt Commun* **505**, 127590 (2022).
220. Mikhaylov D, Zhou BF, Kiedrowski T et al. High accuracy beam splitting using spatial light modulator combined with machine learning algorithms. *Opt Lasers Eng* **121**, 227–235 (2019).
221. Zhang YX, Zhang MK, Liu KX et al. Progress of the computer-generated holography based on deep learning. *Appl Sci* **12**, 8568 (2022).
222. Wu JC, Liu KX, Sui XM et al. High-speed computer-generated holography using an autoencoder-based deep neural network. *Opt Lett* **46**, 2908–2911 (2021).
223. Lee J, Jeong J, Cho J et al. Deep neural network for multi-depth hologram generation and its training strategy. *Opt Express* **28**, 27137–27154 (2020).
224. Hasegawa S, Hayasaki Y. Femtosecond laser processing with adaptive optics based on convolutional neural network. *Opt Lasers Eng* **141**, 106563 (2021).
225. Zhang HH, Hasegawa S, Takahashi H et al. In-system optimization of a hologram for high-stability parallel laser processing. *Opt Lett* **45**, 3344–3347 (2020).
226. Buske P, Völl A, Eisebitt M et al. Advanced beam shaping for laser materials processing based on diffractive neural networks. *Opt Express* **30**, 22798–22816 (2022).
227. Buske P, Hofmann O, Bonnhoff A et al. High fidelity laser beam shaping using liquid crystal on silicon spatial light modulators as diffractive neural networks. *Opt Express* **32**, 7064–7078 (2024).
228. Genty G, Salmela L, Dudley JM et al. Machine learning and applications in ultrafast photonics. *Nat Photonics* **15**, 91–101 (2021).
229. McDonnell MDT, Arnaldo D, Pelletier E et al. Machine learning for multi-dimensional optimisation and predictive visualisation of laser machining. *J Intell Manuf* **32**, 1471–1483 (2021).
230. Wang B, Wang P, Song J et al. A hybrid machine learning approach to determine the optimal processing window in femtosecond laser-induced periodic nanostructures. *J Mater Process Technol* **308**, 117716 (2022).
231. Narazaki A, Yoshitomi D, Takada H et al. ICT data-driven active laser processing. *Photonics Rev* **2024**, 240212 (2024).
232. Mermillod-Blondin A, Burakov IM, Meshcheryakov YP et al. Flipping the sign of refractive index changes in ultrafast and temporally shaped laser-irradiated borosilicate crown optical glass at high repetition rates. *Phys Rev B* **77**, 104205 (2008).
233. Pereiro-García J, García-De-Blas M, De La Rosa P et al. Reconfigurable perfect vortex beam generator based on a liquid crystal spiral phase plate. *Opt Express* **31**, 37653–37662

(2023).
234. Xu A, Nourshargh C, Salter PS et al. Laser-written tunable liquid crystal aberration correctors. *ACS Photonics* **10**, 3401–3408 (2023).
235. Zhao ZM, Chen BH, Salter PS et al. Multielement polychromatic 2D liquid crystal dammann gratings. *Adv Mater Technol* **8**, 2200861 (2023).
236. García-Márquez J, López V, González-Vega A et al. Flicker minimization in an LCoS spatial light modulator. *Opt Express* **20**, 8431–8441 (2012).
237. Clark NA, Lagerwall ST. Submicrosecond bistable electro‐optic switching in liquid crystals. *Appl Phys Lett* **36**, 899–901 (1980).
238. Fukushima S, Kurokawa T, Matsuo S et al. Bistable spatial light modulator using a ferroelectric liquid crystal. *Opt Lett* **15**, 285–287 (1990).
239. Jung W, Kim H, Mishchik K et al. Direct laser patterning of glass mask for micro display using GHz bursts. *J Soc Inf Display* **32**, 426–434 (2024).
240. Ackermann L, Roider C, Schmidt M. Uniform and efficient beam shaping for high-energy lasers. *Opt Express* **29**, 17997–18009 (2021).
241. Matsumoto N, Itoh H, Inoue T et al. Stable and flexible multiple spot pattern generation using LCOS spatial light modulator. *Opt Express* **22**, 24722–24733 (2014).
242. Kaakkunen JJJ, Laakso P, Kujanpää V. Adaptive multibeam laser cutting of thin steel sheets with fiber laser using spatial light modulator. *J Laser Appl* **26**, 032008 (2014).
243. di Pietro VM, Jullien A, Bortolozzo U et al. Thermally-induced nonlinear spatial shaping of infrared femtosecond pulses in nematic liquid crystals. *Laser Phys Lett* **16**, 015301 (2018).
244. di Pietro VM, Bux S, Forget N et al. Phase-only pulse shaper for multi-octave light sources. *Opt Lett* **45**, 543–546 (2020).
245. Barland S, Ramousse L, Chériaux G et al. Reconfigurable design of a thermo-optically addressed liquid-crystal phase modulator by a neural network. *Opt Express* **31**, 12597–12608 (2023).
246. Benstiti A, Bencheikh A, Ferria K et al. Generation of Flexible hyperbolic Airy-like beams using a truncated acousto-optical effect. *Opt Commun* **505**, 127501 (2022).
247. Benstiti A, Bencheikh A, Ferria K et al. Gaussian laser beam structuring using acousto-optic effect: a parametric characterization. *Appl Phys B* **128**, 141 (2022).
248. Miazek A, Dupuy J, Gusachenko I et al. Advanced USP laser process with deep learning and triangular beam shaping for micro Fresnel lenses fabrication. *Proc SPIE* **12408**, 1240802 (2023).
249. Tzang O, Niv E, Singh S et al. Wavefront shaping in complex media with a 350 kHz modulator via a 1D-to-2D transform. *Nat Photonics* **13**, 788–793 (2019).
250. Linden J, Cohen S, Berg Y et al. High-speed temporal and spatial beam-shaping combining active and passive elements. *Opt Express* **29**, 31229–31239 (2021).
251. Li JN, Tang Y, Kuang Z et al. Multi imaging-based beam shaping for ultrafast laser-material processing using spatial light modulators. *Opt Lasers Eng* **112**, 59–67 (2019).
252. Bi J, Wu LK, Li SD et al. Beam shaping technology and its application in metal laser additive manufacturing: a review. *J Mater Res Technol* **26**, 4606–4628 (2023).
253. Badloe T, Lee J, Seong J et al. Tunable metasurfaces: the path to fully active nanophotonics. *Adv Photonics Res* **2**, 2000205 (2021).
254. Berini P. Optical beam steering using tunable metasurfaces. *ACS Photonics* **9**, 2204–2218 (2022).
255. Liu ZX, Zhang BL, Li YK et al. Efficient dynamic tunable metasurface based on $Ge_2Sb_2Te_5$ in the near infrared band. *Appl Opt* **62**, 5508–5515 (2023).
256. Ren HR, Fang XY, Jang J et al. Complex-amplitude metasurface-based orbital angular momentum holography in momentum space. *Nat Nanotechnol* **15**, 948–955 (2020).
257. Emelianov AV, Pettersson M, Bobrinetskiy II. Ultrafast laser processing of 2D materials: novel routes to advanced devices. *Adv Mater* **36**, 2402907 (2024).
258. Han WN, Wei DH, Peng BY et al. 3D femtosecond laser beam deflection for high-precision fabrication and modulation of individual voxelated PCM meta-atoms. *Adv Sci* **12**, 2413316 (2025).
259. Bor Z, Horváth ZL. Distortion of femtosecond pulse fronts in lenses. In Stuke M. *Dye Lasers*: *25 Years* 87–94 (Springer, Berlin, Heidelberg, 1992). doi: 10.1007/3-540-54953-6_6.
260. Patel A, Svirko Y, Durfee C et al. Direct writing with tilted-front femtosecond pulses. *Sci Rep* **7**, 12928 (2017).
261. Sun BS, Salter PS, Booth MJ. Pulse front adaptive optics: a new method for control of ultrashort laser pulses. *Opt Express* **23**, 19348–19357 (2015).
262. Ambat MV, Shaw JL, Pigeon JJ et al. Programmable-trajectory ultrafast flying focus pulses. *Opt Express* **31**, 31354–31368 (2023).
263. Sainte-Marie A, Gobert O, Quéré F. Controlling the velocity of ultrashort light pulses in vacuum through spatio-temporal couplings. *Optica* **4**, 1298–1304 (2017).
264. Froula DH, Palastro JP, Turnbull D et al. Flying focus: spatial and temporal control of intensity for laser-based applications. *Phys Plasmas* **26**, 032109 (2019).
265. Weiner AM. Femtosecond pulse shaping using spatial light modulators. *Rev Sci Instrum* **71**, 1929–1960 (2000).
266. Stoian R, Boyle M, Thoss A et al. Laser ablation of dielectrics with temporally shaped femtosecond pulses. *Appl Phys Lett* **80**, 353–355 (2002).
267. Stoian R, Mermillod-Blondin A, Winkler S et al. Temporal pulse manipulation and consequences for ultrafast laser processing of materials. *Opt Eng* **44**, 051106 (2005).
268. He F, Xu H, Cheng Y et al. Fabrication of microfluidic channels with a circular cross section using spatiotemporally focused femtosecond laser pulses. *Opt Lett* **35**, 1106–1108 (2010).
269. Tan YX, Lv HT, Xu J et al. Three-dimensional isotropic microfabrication in glass using spatiotemporal focusing of high-repetition-rate femtosecond laser pulses. *Opto-Electron Adv* **6**, 230066 (2023).
270. Bor Z, Gogolak Z, Szabo G. Femtosecond-resolution pulse-front distortion measurement by time-of-flight interferometry. *Opt Lett* **14**, 862–864 (1989).
271. Bor Z, Racz B, Szabo G et al. Femtosecond pulse front tilt caused by angular dispersion. *Opt Eng* **32**, 2501–2504 (1993).
272. Akturk S, Gu X, Zeek E et al. Pulse-front tilt caused by spatial and temporal chirp. *Opt Express* **12**, 4399–4410 (2004).
273. Yang WJ, Kazansky PG, Svirko YP. Non-reciprocal ultrafast laser writing. *Nat Photonics* **2**, 99–104 (2008).
274. Chambonneau M, Grojo D, Tokel O et al. In-volume laser di-

rect writing of silicon —challenges and opportunities. *Laser Photonics Rev* **15**, 2100140 (2021).

Acknowledgements

This was supported by the French ANRT agence nationale de la recherche technologique under the CIFRE conventions industrielles de formation par la recherche framework.

Competing interests

The authors declare no competing financial interests.